

**MECHANISMS OF URINARY STONE
FRAGMENTATION USING
THE HO:YAG LASER**

By

JONG-EUL LEE

Bachelor of Science

Dongguk University

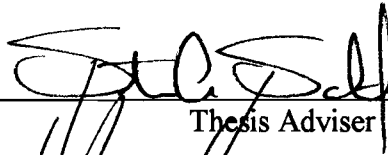
Seoul, Korea

1991

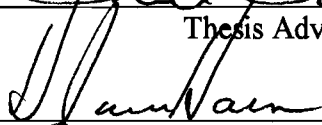
**Submitted to the Faculty of the
Graduate College of the
Oklahoma State University
in partial fulfillment of
the requirements for
the Degree of
MASTER OF SCIENCE
December, 1995**

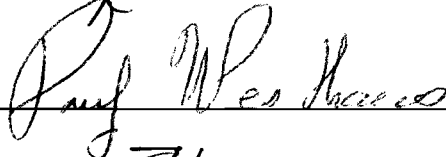
MECHANISMS OF URINARY STONE
FRAGMENTATION USING
THE HO:YAG LASER


Thesis Approved:



Thesis Adviser







Dean of the Graduate College

ACKNOWLEDGMENTS

I wish to express my sincere appreciation to my major advisor, Dr. Steven Schafer for his intelligent supervision, constructive guidance, inspiration and friendship. My sincere appreciation extends to my other committee members Dr. Paul Westhaus and Dr. James Harmon, whose assistance, encouragement, and friendship are also invaluable.

More over, I wish to express my sincere gratitude to Dr. Jin-Fu Zhou who provided suggestions and assistance for this study.

I would also like to give my special appreciation to my parents for their support and encouragement.

Finally, I would like to thank the Department of Physics, the Noble Research Center, and the Presbyterian Health Foundation for support during these two years of study.

TABLE OF CONTENTS

Chapter	Page
I . INTRODUCTION	1
Background	1
Review of the Literature	1
Introduction of ESWL	2
Introduction of Laser-Induced Shock Wave Lithotripsy	2
The Characteristics of the Ho:YAG Laser	3
Mechanisms of Urinary Stone Fragmentation Using the Flash-Lamp-Pumped Tunable Dye Laser	3
The Characteristics of Pulsed-Dye Laser Lithotripsy for Urinary Stones	4
Introduction of Techniques Using a Pulsed-Dye Laser and a Scanning Diode Array	5
Introduction of Biliary Stones	6
Comparison of Biliary Stone Fragmentation Using the Pulsed-Dye and Ho:YAG Lasers	7
Mechanisms of Biliary Stone Fragmentation Using the Pulsed-Dye Laser	7
Mechanisms of Biliary Stone Fragmentation Using the Ho:YAG Laser	7
Logical Assumptions	7
Purpose of the Study	8
Scope and Limitations	8
II . MATERIALS AND METHODS	8
Chapter Overview	8
Methodology of Visual Observation of Fragmentation	8
Observation of Vapor Bubbles	9
Evolution of Vapor Bubbles	10
Measurement of Bubble Size	10
Normal Incidence Experiment	10
Tangential Incidence Experiment	11
CH ₃ CN and Benzene Experiments	12
Methodology of Fragmentation Rate of Urinary Calculi	12
Methodology of Reflectivity of Urinary Stones	13

Chapter	Page
III. RESULTS	15
Visual Observation of Fragmentation	15
Fragmentation Rate of Urinary Calculi	19
Reflectivity of Urinary Stones	20
IV. DISCUSSION	21
Summary	21
Comparison with Results of Other Workers	21
Conclusions	22
Concluding Comment	23
REFERENCES	50

LIST OF TABLES

Table	Page
1. Fragmentation Thresholds vs Wavelength	24
2. Fragmentation Thresholds vs Pulse Duration	24
3. Fragmentation Thresholds vs Fiber Diameter	24
4. Fragmentation Thresholds Values for Different Types of Biliary Stones	25
5. The List of Urinary Stones	26
6. Average Values of Bubble Size	27
7. Fragmentation Distances of Urinary Stones Using the Ho:YAG Laser at a Fixed Power of 2 W (Normal Incidence case)	28
8. Description of Fragmentation Process of Urinary Stones Using the Ho:YAG Laser	29
9. Fragmentation Rates of Urinary Stones at 2, 5, and 8 W for 15 Seconds Using the Ho:YAG Laser	30
10. Reflectivity of Urinary and Biliary Stones at a Fixed Laser Power of 3 W	31
11. Average Reflectivity of Stones for the Ho:YAG Laser Light at 3 W	32
12. Fragmentation Mechanism of Urinary Stones Using the Ho:YAG Laser	33
13. Comparison of Urinary Stone Fragmentation Using the Pulsed-Dye and Ho:YAG Lasers	34

LIST OF FIGURES

Figure	Page
1. Schematic Representation of Stone Fragmentation Using ESWL Devices	35
2. Spectrum from a Cystine Stone by Pulsed-Dye Laser	36
3. Spectrum from a CHPD Stone by Pulsed-Dye Laser	36
4. Spectrum Showing Reflection of Pulsed-Dye Laser Light from Surface of a Stone	36
5. Schematic Illustration of the Equipment of Visual Observation	37
6. The Evolution of Vapor Bubbles at 2 W Pulses while Varing the Lengths of Delay (20 μ S - 320 μ S)	38
7. Schematic Representation of Stone Ablation with the Ho:YAG Laser	39
8. Schematic Representation of Stone Ablation in Tangential Incidence	40
9. Schematic Illustration of the Reflectivity Apparatus	41
10. The Reflectivity of Urinary and Biliary Stones (> 80 % cholesterol) lied between 10 % and 99 % for the Ho:YAG Laser Light ($V_2 / V_1 = r$)	42
11. Schematic Representation of a Typical Ho:YAG Laser-Induced Vapor Bubble in Water at a Flash Delay of 170 μ S	43
12. Fragmentation Rate of Urinary Stones at a Pulse Repetition Rate of 15 Hz and a Fixed Power of 2 W for 15 Seconds	44
13. Fragmentation Rate of Urinary Stones at a Pulse Repetition Rate of 15 Hz and a Fixed Power of 5 W for 15 Seconds	45
14. Fragmentation Rate of Urinary Stones at a Pulse Repetition Rate of 15 Hz and a Fixed Power of 8 W for 15 Seconds	46

Figure	Page
15. Fragmentation Rate of Urinary Stones at a Pulse Repetition Rate of 15 Hz and Powers of 2, 5, 8 W for 15 Seconds	47
16. Comparisons of the Fragmentation Rate and the Reflectivity of Urinary Stones Using the Ho:YAG Laser	48
17. Comparisons of the Fragmentation Distance and the Reflectivity of Urinary Stones Using the Ho:YAG Laser	49

I . INTRODUCTION

Urinary stones, or calculi, located in the kidney, in the ureter which conveys the urine from the kidney to the urinary bladder, or in the urinary bladder are the most common disorder of the urinary tract (1, 2). Urinary stones arise from a transient, intermittent or permanent disorder in urine components (4) that induces a certain concentration of nucleating material by urine supersaturation with the salt of a stone-forming crystal (3). Absence or low concentration of some urinary substances (eg., magnesium, pyrophosphate, citrate, and various peptides) permits crystal formation of the stones (3). The first stage in stone formation is nucleation initiated by concentration of a small quantity of urine components in the core of a stone, followed by growth around the initial nucleus (4). Urinary stone components may be mineral, organic, or both. More than 65 different molecules have been so far found in urinary calculi (4, 5). Considering an origin of the cause of urinary stones, four groups of urinary stones are usually distinguished : calcium stones, uric acid stones, infection stones, and cystine stones (4). Many researchers have considered “ calcium stones ” as a unique class of stones, although this class actually includes various molecular compounds (calcium oxalate (CaOx), calcium phosphate (CaP), magnesium and calcium phosphate). Moreover, these components may be present in different crystalline phases both for CaOx [calcium oxalate monohydrate (whewellite), calcium oxalate dihydrate (weddellite), and, rarely, calcium oxalate trihydrate], and CaP [carbonate apatite (carbapatites), amorphous CaP , octacalcium phosphate, dicalcium phosphate dihydrate (brushite)]. Usually, the group of infection stones is defined to include stones which contain magnesium ammonium

phosphate hexahydrate (struvite) and which result from chronic urinary tract infection with urea-splitting bacteria inducing urinary diversion (3, 4).

Urinary stones may be treated by several lithotripsy techniques. Among the lithotripsy techniques, extracorporeal shock wave lithotripsy (ESWL) was introduced in the early 1980s. Urinary calculi can be treated with extracorporeal shock wave lithotripsy (ESWL) without open surgery. The contact of a shock wave (a high-energy pressure wave) generated in water (by electrohydraulic, piezoelectric, or electromagnetic devices) by the abrupt release of energy in a small space with a stone produces a compression wave along the front surface of the stone, causing the anterior surface to crumble. As the shock wave traverses to the posterior surface of the stone, part of the wave is reflected, creating tensile stress and fragmentation along this surface [see Fig. 1]. Shock waves focused on the stone repeatedly finally reduce it to numerous small fragments that can be passed spontaneously (6). Generally ESWL is not useful in treating ureteric stones which cause severe obstruction to the ureter (7) because imaging or focusing on the stones with ESWL may be precluded by extreme obesity (8).

Over the past decade, minimally invasive laser-induced shock wave lithotripsy has been implemented endoscopically in the treatment of ureteral calculi. Laser lithotripsy since its advent has been shown to be a harmless and effective method of urinary calculi fragmentation (8). Generally speaking, laser energy influences only the stone that absorbs it ; the stone which absorbs the laser energy is vaporized enough to induce a plasma at its surface, by which a shock wave is generated that fragments the stone. Accordingly, the energy acts only on the stone and not on surrounding tissue. Although the argon, neodymium YAG, and carbon dioxide lasers have played an important role in

various field of medicine, urinary stone fragmentation using these devices has not been very successful (8). Each laser, operating at a specific wavelength, emits a continuous beam that has the effect of heating the target material (9). Thermal changes due to constant energy do not cause the fragmentation of urinary calculi but instead cause vaporization of the surface because continuous wave lasers create constant energy (2000 to 3000 °C) enough to vaporize the urinary calculi (8). Recently, a flashlamp-pumped pulsed holmium:YAG laser that emits in the near infrared region (2100 nm) has aroused the interest of urologists because of the high optical absorption of water ($\alpha = 30 \text{ cm}^{-1}$) (17, 20) at that wavelength and because 2100 nm radiation is readily transmitted through silica optical fibers with negligible power attenuation (0.039 dB/km) (10). Thus it may be expected that the Ho:YAG laser may be applied in the fragmentation of urinary stones. The availability of Ho:YAG lasers having an adequate optical fiber system has been a considerable stimulus to research in laser lithotripsy of biliary and urinary calculi (16). By measurement of the fragmentation rate and reflectivity of stones, in addition to visual observation, the fragmentation of urinary stones using the Ho:YAG laser has been analyzed and compared to lithotripsy using the pulsed-dye laser and to biliary stone lithotripsy using the Ho:YAG laser. The physical mechanisms of stone fragmentation are expected to be different in the three cases because of the different stone components and characteristics of the lasers used for the fragmentation of stones.

For laser lithotripsy with a flash-lamp-pumped tunable dye laser in the treatment of urinary calculi, the fragmentation mechanism is described as arising from the formation and collapse of a plasma at the calculi surface (8). The high temperature plasma, a fast expanding cavity of ions and electrons, is formed by the absorption of laser light by the

calculi. When the plasma rapidly collapses after its expansion, a shock wave is produced, which gradually fragments the calculi. This model suggests that the fragmentation rate depends on the component and size of the calculi because the laser energy affects only the stone that absorbs it. Calculi composed of calcium oxalate dihydrate, magnesium ammonium phosphate hexahydrate and uric acid fragment more easily than those of calcium oxalate monohydrate, cystine and calcium phosphate.

When the pulsed-dye laser is used in the treatment of urinary calculi with a quartz optical fiber, carrying the pulsed-dye laser light, in contact with urinary calculi, the fragmentation threshold (the minimum energy per pulse required to produce fragmentation) is least at the laser wavelength of 445 nm, at the shortest pulse duration and at the narrowest fiber diameter, (11) [see Table 1, 2, 3: (11)]. Thus, the fragmentation depends on the absorption of laser light and the power density (inversely related to the square of fiber diameter). The attenuation (the fiber intrinsic loss) in the fiber at the laser wavelengths of 445 nm, 504 nm, and 577 nm is approximately 19.38 dB/km, 11.78 dB/km, and 6.86 dB/km, respectively (12). From this research, it was reported that, in particular, the energy per pulse generating fragmentation when the fiber is in contact with the stone has no fragmentation effect if the fiber is withdrawn from the stone surface by 3 mm. The divergence of the laser beam, which is dependent on the fiber diameter is quite important in view of minimizing the energy required to cause fragmentation to avoid tissue damage because the fragmentation threshold is least at the narrowest fiber diameter. There are various mechanisms that cause tissue damage by a misaimed laser pulse or stray laser radiation. In particular, absorption that leads to tissue damage may occur as the laser energy is transferred into heat energy within various

tissues.

Using a pulsed-dye laser ($\lambda = 504 \text{ nm}$) and a scanning diode array in an in vitro study, Holden et al. analyzed the components of the urinary calculi. They found that most components can be distinguished by the differences in their individual spectra (13). Even though it was difficult to obtain spectra from cystine and calcium hydrogen phosphate dihydrate stones [see Fig. 2, 3], the spectra were emitted when an acoustic “ crack ” was heard as the laser energy was absorbed in the stone surface. The spectrum consisted purely of the laser light reflection from the stone surface [see Fig. 4] is clearly different from the spectra obtained from the cystine and calcium hydrogen phosphate dihydrate stones because no “ crack ” is audible at pure reflection of the laser light from the stone surface. In this experiment, an analysis fiber whose other end was inserted into the entry port of a scanning photo-diode array was positioned adjacent to a laser fiber as the laser light was fired through the laser fiber above a stone surface. Resulting optical spectra was recorded first on a digital storage oscilloscope connected to the output from the diode array and then on an X-Y plotter coupled with the oscilloscope. The main feature of this technique is rapid identification of the stone components in vivo. These results obtained by using a pulsed-dye laser with a scanning diode array suggests that the fragmentation is dependent not only on the hardness of the stone but also the characteristics of stone surface. Stones with a dark surface fragment more easily than those with a pale surface because the former absorbs the laser energy better than the latter (13). Thus, the resultant fluorescent emission of the stones, recorded using the pulsed-dye laser with a scanning diode array, appeared to be related to the stone components which absorb the laser beam. At shorter pulse durations, the pulsed-dye laser needs less total energy to

fragment urinary stones because the pulse duration inversely influences the maximum shock (proportional to peak power density) (14). Generally the relationship among energy, time and power can be expressed by follows.

$$\text{Energy} = [\text{power}] [\text{time}] \text{ or } 1 \text{ Joule} = [1 \text{ watt}] [1 \text{ second}]$$

Using the equation above,

$$\text{Power} = \text{energy} / \text{time} \text{ or } 1,000 \text{ watts} = 1 \text{ mJoule} / 1 \mu\text{sec.}$$

defines how pulse duration inversely affects peak power (or power density). Thus the fragmentation threshold (the minimum energy required to fragmentation) depends proportionally on the pulse duration. For lithotripsy of uric acid stones, the highest amount of laser energy is needed for fragmentation because the stones have concentric and radial laminations (14, 15). Even though the uric acid stone fragments relatively easily, the highest amount of energy is required for fragmentation because the laser fragments each layer separately.

Biliary stones located in the gallbladder or the bile duct are a heterogeneous group, varying in bile pigment, cholesterol and calcium salt content. Black stones are known as “pigmented stones” and composed mainly of calcium bilirubinate. White or pale tan “cholesterol stones” are composed of cholesterol monohydrate and “brown” or “mixed stones” are a variable mixture of pigment and cholesterol stones plus calcium salts, bile pigments, proteins, fatty acids, and bile acids (16).

Spindel et al. (16) reported that the fragmentation threshold required to induce fragmentation of biliary calculi with the flashlamp pumped dye laser ($\lambda = 640 \text{ nm}$) varied notably for cholesterol (white), light brown, dark brown and pigmented stones, whereas the fragmentation threshold required to induce fragmentation with the Ho:YAG ($\lambda =$

2100 nm) laser was approximately equal for all types of biliary stones. They determined that the dye laser emitting at the visible wavelength produces fragmentation at lower fragmentation threshold, but the parameters to produce fragmentation vary considerably for different types of stones. In contrast, the Ho:YAG laser emitting at the near infrared wavelength requires a higher fragmentation threshold but the parameters for efficient fragmentation are almost the same for all types of biliary stones [see Table 4]. Thus, it is not necessary to identify stone type when the Ho:YAG laser is used to fragment stones. In addition, the dye laser may cause serious damage to surrounding tissues and can cause damage to the tip of optical fiber unless it is considered that the fragmentation parameters vary significantly for different types of stones.

Teng et al. (17, 18, 19) proposed the first model describing a mechanism of biliary stone fragmentation with the pulsed-dye laser. Their results suggest that a small portion of stone substance is vaporized and ionized as the absorption of laser light by the stone occurs , which induces the formation of a plasma at the stone surface. The plasma then continues to absorb the subsequent laser light, expands rapidly and generates a strong acoustic wave with high pressure into the stone and into the surrounding fluid medium. This acoustic shock wave induces the stone to fragment gradually. Because of the high temperatures of the plasma, energy loss by thermal reradiation may be significant. In addition, the evolution of the plasma and the generation of the acoustic wave are considerably affected by the surrounding fluid.

Schafer et al. (17) suggested a mechanism for Ho:YAG laser lithotripsy of biliary stones, which is considerably different from the one proposed by Teng et al. for laser lithotripsy with the visible pulsed-dye laser. Their model proposes that stone

fragmentation begins with absorption of the laser beam by the water surrounding the stone, which causes the formation and collapse of a vapor bubble. The remainder of the laser beam is absorbed by the stone, causing the stone to melt and emit the stone material from the surface. The ejected material subsequently resolidifies and is swept away by the water vapor bubble. This model is consistent with their experimental investigations and further developed than the one by Teng et al. However, there is little information available on urinary stone fragmentation using the Ho:YAG laser. As it was mentioned previously that urinary stone fragmentation using the Ho:YAG laser was expected to be different from fragmentation using the pulsed-dye laser and even gallstone fragmentation using the Ho:YAG laser, we presumed that the physical mechanisms of stone fragmentation would differ in the three cases.

The purpose of this research was to investigate the fragmentation of urinary stones using the Ho:YAG laser in order to determine the physical mechanism of stone fragmentation. This study may lead to a better understanding of an interaction between the Ho:YAG laser light and urinary stones.

II. MATERIALS AND METHODS

We classified human, canine, porcine, equine, and feline urinary calculi by their predominant constituents and selected human and equine stones for preliminary stone fragmentation using the Ho:YAG laser. The resulting 10 types of stones were named by the main chemical components as calcium oxalate monohydrate, calcium oxalate dihydrate, tricalcium orthophosphate, ammonium acid urate, calcite, uric acid, calcium phosphate, calcium hydrogen phosphate dihydrate, cystine, magnesium ammonium

phosphate hexahydrate (hereafter referred to as, respectively, COM, COD, TO, AAU, Calcite, UA, CP, CHPD, Cystine, MAPH) [see Table 5].

Our preliminary examination of urinary stone fragmentation using the Ho:YAG laser showed the existence of a “ tic ” sound without any visible emission at the tip of the fiber in contact with the stone. Even when the laser was fired into plain water, we heard the same sound without any glow. After these initial observations, we performed visual observation of fragmentation, and measured fragmentation rate and reflectivity of stones with the Ho:YAG laser in order to understand the mechanisms of urinary stone fragmentation.

A. Visual observation of fragmentation

The Ho:YAG laser emitting at a wavelength of 2100 nm has the ability to produce vapor bubbles in plain water, regardless of the presence of a stone, because the 2100 nm wavelength is strongly absorbed by water ($\alpha = 30 \text{ cm}^{-1}$). The formation of a vapor bubble in water is initiated by an evaporative process due to absorption of the laser light in water. Understanding the formation of the bubble plays a key role in understanding the mechanism of urinary stone fragmentation with the Ho:YAG laser.

We observed the vapor bubbles using the experimental setup shown in Fig. 5. The Ho:YAG laser used in these investigation was the Sunrise Technologies sLase 210 laser operating at 2100 nm with maximum average power of 15 watts (W). The pulse repetition rates are selectable from 5 to 20 pulses / second (Hz) generating integrated output pulses of 250 - 350 μS duration. This optical device is an example of a pulsed mode laser, generating pulses of 100 - 1000 mJ. For each pulse, there are a great number

of submicrosecond spikes ; these spikes (each spike 100 nS - 1 μ S long) are too closely spaced and too numerous to be completely resolved with an IR photodetector. A

Polymicro Technologies FLP 320 / 385 / 415 optical fiber with 320 μ m core diameter was coupled to the output of the laser. A portion of the laser light passing through this optical fiber was split off and transmitted to a Judson J10 InSb photodetector, using a glass microscope slide as a beam splitter. The remainder of the laser light was sent to a second fiber, which was inserted into a water tank. Approximately 50 % of the laser pulse was lost to the beam splitter and coupling lenses. By coaxial cable, the signal from the IR photodetector was carried to a Hewlett - Packard HP8112A delay generator, whose output controlled an EG & G Electro-Optics 549 Microflash. This flash with 500 nS pulse duration served as the light source for visual observation, emitting a white light pulse. A stereomicroscope (20 X magnification) was positioned in front of the small water tank to observe the vapor bubble and the fragmentation process.

In order to observe the development of vapor bubbles over the course of their expansion and collapse in plain water, the optical fiber coupled with the Ho:YAG laser was inserted normally into the water tank. By means of varying the length of delay (20 - 320 μ S) provided by the delay generator while firing a series of 2 W pulses, we ascertained that the vapor bubbles could be clearly observed at a flash delay of 170 μ S [see Fig. 6]. When we varied the length of delay by 50 μ S from 20 - 320 μ S, the vapor bubbles became brighter and larger until 170 μ S and, after 170 μ S, the vapor bubbles gradually became dimmer and smaller. At a flash delay of 320 μ S, we couldn't observe the vapor bubbles because the vapor bubbles had collapsed.

We also measured the sizes of bubbles in the presence of stones, to determine if

the sizes of bubbles were related to stone types. The stone was fastened to a small stand, using hot-melt glue, placed in the water tank, and the Ho:YAG fiber was placed normally to the stone's surface by a three-dimensional translation stage [see Fig. 7 (a)]. Using a micrometer with the three dimensional translation stage, we set the zero point on the basis of when the fiber was placed in direct contact with the stone's surface, and attempted to move the fiber tip up from the stone's surface until the bubbles barely touched ($0 \leq d \leq 0.1 \text{ mm}$) the stone's surface while firing a series of 2 W pulses at a flash delay of 170 μS . The bubble size was obtained by adding the distance between the fiber tip and the stone's surface to the one between the bubble's top and the fiber tip [see Fig. 7 (a)].

We repeated the experiment with the optical fiber placed normal to the stone's surface to obtain the fragmentation threshold distance defined as the distance between the fiber tip and the stone's surface at the moment fragmentation of the stone begins to occur. In addition, we observed how the stones were fragmented by the laser light using the microflash technique mentioned formerly with 20 X magnification and described the course of fragmentation events of the stones. When we placed the optical fiber closer to the stone's surface while firing the laser, fragmentation was caused by absorption of laser energy by the stone, which varied according to stone types, as expected.

In order to ascertain if ablation of the stone was the result of absorption of laser light by the stone, the optical fiber was positioned approximately tangential to the stone's surface [see Fig. 7 (b)]. In this case, the cone of light [see Fig. 7] extending through the vapor bubble was not intercepted by the stone's surface until the fiber was moved close to the stone. We attempted to cut the stone's surface in a circular shape with a razor blade and positioned the optical fiber tangentially to the stone's arc while firing a

series of 2 W pulses [see Fig. 8]. When we placed the fiber closer to the stone's surface, some stones began to fragment, ejecting broken particles but others did not.

In an attempt to determine the influence of vapor bubble on fragmentation of stones, we generated bubbles which barely touched the stone's surfaces at normal incidence when firing the laser light. Mechanical forces generated at the vapor-liquid boundary on the bubble was also considered as an explanation of the origin of the stone fragmentation, together with direct absorption of the laser light by the stone. We also performed the experiment using a liquid which has negligible optical absorption at 2100 nm, so that no vapor bubble was formed. To test this, we used acetonitrile (CH_3CN) which exhibits little absorption at 2100 nm ($\alpha = 0.88 \text{ cm}^{-1}$) (17) in lieu of the water in the small tank. We repeated the same experiment even in benzene, which also has little absorption at this wavelength ($\alpha < 0.01 \text{ cm}^{-1}$) (21). Furthermore, these results were compared with the data from scanning electron microscopy of urinary calculi.

B. Fragmentation rate of urinary calculi

Fragmentation rate is defined as the mass difference of stones before and after fragmentation per unit time of exposure to the laser light. Using a laboratory balance, we measured stone mass M_1 before its fragmentation, and we attempted to fragment stones using the Ho:YAG laser at 2, 5 and 8 watts (W) average power for 15 seconds (T) at a pulse repetition rate of 15 Hz. Taking the stone out of the water tank after finishing the fragmentation, we dried it for 10 - 12 hours using a fiber optic light lamp with output of 150 W and measured its mass M_2 . Thus the fragmentation rate was expressed by $(M_1 - M_2) / T$ (gram / sec) at 2, 5, and 8 watts. By these measurements, we could

investigate if the fragmentation rate was directly related to the absorption of the Ho:YAG laser light by urinary stones from the fact that the energy affects only the material that absorbs it.

C. Reflectivity of urinary stones for the Ho:YAG laser light

We attempted to apply published data from infrared spectroscopy on urinary calculi to our study in order to obtain information on the dependence of absorption on stone components for Ho:YAG laser light. Infrared spectroscopy which has been used to identify chemical compounds uses a length of ceramic tube heated by an internal metallic element to about 1200 °C as the source of illumination (22). The radiant energy produces a continuous spectrum (4000 - 200 cm^{-1}) which induces oscillations in crystals. The absorption bands generate a typical spectrum for each chemical compound when the energy is absorbed by a sample material. However, the bands 4000 - 200 cm^{-1} of this infrared spectroscopy corresponded to wavelengths of 2500 - 50000 nm. Because this absorption band of infrared spectroscopy was at a longer wavelength than the 2100 nm output of the Ho:YAG laser, we were unable to apply this technique to our experiments.

Instead of using infrared spectroscopy , we made reflectivity measurements using an integrating sphere, from Labsphere Laser Power Measurement Systems, along with Spectralon diffuse reflectance standards, to obtain the reflectivity of urinary calculi and biliary calculi for the Ho:YAG laser light. We measured the reflectivity of stones using the apparatus shown in Fig. 9. The integrating sphere is the ideal equipment for measuring the total power of a beam of radiation (23). The input flux is spatially integrated and

measured by a photodetector positioned on the sphere wall. We used two reflectance standards of 99 % (white standard) and 10 % (gray standard) having known reflectivity. The beam coming out of the fiber, shown in the Fig. 8, was separated and a portion sent to a photodetector, using a beam splitter. The rest of the laser light was focused into a second fiber, which was inserted into the integrating sphere. We placed a 99 % reflectance standard first under the integrating sphere. Using a Hewlett - Packard HP54504A digital oscilloscope, we measured the power V_1 (mV) of the laser output monitored by the detector and simultaneously determined the power V_2 (mV) of the beam output integrated by the sphere following reflection by the reflectance standard. Subsequent to this step, we repeated the same experiment for a 10 % reflectance standard, and then for powdered stones. To collect the laser beam reflected by the stone into the the integrating sphere without any energy loss by deviation of the laser light caused by the uneven surface of the stone, we ground the stone to powder, using mortar and pestle, poured the powder into a small container, and made the surface of the powder level.

Generally, the ratio of V_2 / V_1 of 99 % reflectance standard and that of 10 % reflectance standard are maintained to be identical in every case of measurements. Our experiment showed that the average V_2 / V_1 of the 99 % standard was about 3.50×10^{-3} and that of 10 % standard was about 2.04×10^{-3} [see Table 10]. Assuming that the reflectivity of stones for the Ho:YAG laser light is between 10 % and 99 %, we measured V_2 / V_1 of the stone and compared it to 3.50×10^{-3} and 2.04×10^{-3} in order to obtain the reflectivity of stones [see Fig. 10]. If r is V_2 / V_1 of the stone and R is the reflectivity of the stone, R can be expressed by follows.

$$99 \% \text{ reflectance standard} : V_2 / V_1 = 3.50 \times 10^{-3}$$

$$10 \% \text{ reflectance standard} : V_2 / V_1 = 2.04 \times 10^{-3}$$

$$R \% (\text{ reflectivity of stones }) : V_2 / V_1 = r$$

$$\rightarrow 99 - 10 : 3.50 - 2.04 = R - 10 : r - 2.04$$

$$\rightarrow 89 : 1.46 = R - 10 : r - 2.04$$

$$\rightarrow 1.46 (R - 10) = 89 (r - 2.04)$$

$$\therefore R = 89 \{ (r - 2.04) / 1.46 \} + 10$$

$$\text{where } r = V_2 / V_1, (2.04 \times 10^{-3} \leq r \leq 3.50 \times 10^{-3}, \text{ neglect } 10^{-3})$$

III. RESULTS

A. Visual observation of fragmentation

We observed the evolution of vapor bubbles in plain water by varying the length of delay of the strobe flash from 20 to 320 μS . Fig. 11 displays a typical vapor bubble in plain water described by observation using the experimental setup shown in Fig. 5. The vapor bubble was first observable at a delay of 70 μS and revealed its shape relatively clearly at a delay of 170 - 220 μS . The vapor bubble was considerably nonspherical, as has been described previously for a Ho:YAG laser - induced vapor bubble in water (17). This nonspherical bubble is caused by the relatively long duration of the laser pulse (250 - 350 μS). Laser light passing through the water vapor in the vapor bubble can reach the vapor - liquid boundary at the lower end of the bubble with negligible attenuation (fiber attenuation at 2.1 μm is 0.039 dB/km). Additional evaporation occurs at this boundary, due to absorption of the laser light by the water. This result is compared to previous research (24) for laser-induced vapor bubbles which have been spherical, due

to short pulse duration. Using a micrometer attached to a three - dimensional translation stage, we measured the values of bubble size in the presence of urinary stones. Table 6 shows the average values of bubble size obtained as the fiber tip was positioned over the stone's surface by 1 mm. The average values of bubble size were 0.8 ± 0.07 mm and nearly the same regardless of the stone type. The size of the vapor bubble is independent of the stone types and the laser power because the vapor bubble is formed when the laser light is absorbed by water.

By measurement of fragmentation distances (d) at the moment fragmentation of the stone begins to occur, according to stone type, we found that cystine, calcite, UA ($0.76 \text{ mm} \leq d \leq 1.0 \text{ mm}$) fragmented more easily than COM, COD, UA, AAU, CP, CHPD, MAPH, TO ($0 \text{ mm} \leq d \leq 0.4 \text{ mm}$) [see Table 7]. We realized that these fragmentation distances were less than or roughly close to the bubble size obtained above. It appears that fragmentation of the stone begins only if the optical fiber is close enough that the vapor bubble generated by the laser light touches the stone's surface. We inferred that the origin of the fragmentation was direct absorption of the laser energy by the stone or acoustic pressure generated at the vapor - liquid boundary of the bubble. By making the bubble barely touch the stone's surface when firing the laser, cystine, UA, calcite stones started to fragment but COM, COD, AAU, CP, CHPD, TO, MAPH were hardly broken since the fragmentation distance of these stones is much shorter than the bubble size. By varying the distance ($0 - 3 \text{ mm}$) between the fiber tip and the stone's surface at a fixed power of 2.0 W, TO, CHPD, MAPH (stones hardly broken by the Ho:YAG laser light) had fragmentation distances of 0.15, 0.16, 0.21 mm, respectively. By varying the laser power ($1 - 15 \text{ W}$) while keeping the fiber distance fixed at 3 mm, these stones

hardly fragmented. These findings suggest that the distance from the fiber tip to the stone's surface has more important effect upon efficient fragmentation of the stone than the laser power. From the fact that the divergence angle of the beam is 23° for the fiber we used, moving the fiber tip closer to the stone's surface causes the laser pulses to be absorbed in a smaller area on the stone's surface. The concentration of the laser energy results in increased absorption of the laser energy by the stone. Because the ablation of the urinary stone by the laser having an output wavelength of 2100 nm is able to occur by direct absorption of the laser light by the stone's surface, it may be necessary to fragment the stone at a distance less than the bubble size or nearly so in order to allow the absorption of laser light by the stone.

To determine this more definitely, we repeated the experiment using tangential incidence of the laser light to the stone's surface. We observed no ablation (with minor erosion after many laser pulses). No ablation occurred until the cone of light [see Fig. 7 (a)] moving through the vapor bubble touched the stone's surface, when the fiber was moved close enough to the stone. The absorption of the laser light by the stone might be required for ablation even though the absorption of the laser light differed according to stone types (which will be discussed later in the reflectivity experiment).

In an attempt to ascertain whether the vapor bubble might also be responsible for ablation, we replaced the water in the small tank with acetonitrile (CH_3CN) which showed little absorption at 2100 nm ($\alpha = 0.88 \text{ cm}^{-1}$). It appeared that cystine (melting point, 260°C) and UA melted when irradiated through acetonitrile while other stones showed very little effect. By moving the fiber close to the surface of the stones composed of cystine and UA, the stones had a few air bubbles on the surface due to temperature rise,

were melted, and resolidified in large globules, which adhered to the stone and to the fiber. After 3600 - 4500 pulses of the laser, the stones tended to appear burnt having a black color on the surface. It is not clear whether this effect is caused by the chemical components of the stone reacting to the laser beam, or resolidified globules adhered to the stone being burnt by subsequent laser pulses. In the case of biliary stone fragmentation using the Ho:YAG laser, the melting effect tended to be same for all stones because all biliary stones contain cholesterol (m.p., 150 °C). However, in the case of urinary stone fragmentation using the Ho:YAG laser, some stones exhibited the melting effect but others did not since the components of the stone varied with stone type. Our results showed that calcite, cystine and UA stones fragmented more easily than other urinary stones. It was noticeable that the calcite stone (m.p., 1339 °C) fragmented easily even if it couldn't be melted by the laser energy. We imagined that the calcite stones fragmented by direct absorption of the laser energy by the stone, not by melting the stone but by inducing thermal expansion of the stone, or by acoustic pressure generated at the vapor - liquid boundary of the vapor bubble. In particular, the UA stone, as mentioned before, tended to fragment easily using the pulsed dye laser even if the highest amount of energy was needed due to the stone structure of concentric and radial laminations. On the other hand, without the highest amount of energy, the UA stone fragmented well using the Ho:YAG laser because the urinary stone fragmentation depended not on the laser power but on the absorption of the laser energy by the stone even though the unique feature of the UA stone structure needed many tens of pulses (18000 - 27000 pulses) to fragment. Because the ablation from temperature rise by the absorption of the laser energy differed according to stone types, some stones (cystine, UA) had melting effect which leads to the

fragmentation of the stones but other stones didn't have melting effect even if they fragmented by the absorption of the laser energy.

We also attempted to perform ablation experiments using benzene, whose optical absorption at 2100 nm was less than that of water. The result was the same as in the experiment using acetonitrile. Thus, the vapor bubble explicitly contributes to the fragmentation of the stone.

Using the microscope technique, we observed the fragmentation processes of urinary stones and obtained descriptions of visual observation of stone fragmentation [see Table 8]. The stones which interact well with the Ho:YAG laser light, (calcite, cystine) tended to have smooth surface without lamina, which didn't require the highest amount of energy to fragment the stones while those which were hardly broken, (COM, TO, AAU, CHPD) were likely to have a hard surface with inner nuclei which didn't interact well with the laser energy. Even though UA could fragment relatively easily, many tens of pulses were required because it contained inner radial nuclei. We might imagine that the fragmentation of urinary stones could be influenced by the surface structure of the stones after the laser light was absorbed by the stones.

B. Fragmentation rate of urinary calculi

Table 9 displays fragmentation rate of urinary stones, using the Ho:YAG laser which generates pulses of 2, 5, 8 W at pulse repetition rate of 15 Hz for 15 seconds. Calcite had the highest fragmentation rate among the urinary stones. Even though cystine and uric acid stones were easy to fragment, the fragmentation rate was not high because the size of ejected fragments was much smaller than those of calcite stones. On the other

hand, COM, TO and CHPD were so hard to fragment that the fragmentation rates were significantly low ; in addition the size of the fragments was also very small. The size of the fragments might be the important parameter to decide the fragmentation rate [see Fig. 12, 13, 14, 15]. From the fact that the calcite stone has the highest fragmentation rate even though its color is yellowish white, we see that the urinary stone fragmentation with the Ho:YAG laser is not related to the stone's visible color but to its absorption at 2100 nm. For urinary stone fragmentation with a pulsed dye laser, the stones with a dark surface fragment well due to high absorption of the laser energy, whereas those with a pale, reflective surface absorb little energy and fragment poorly (13). In summary, the fragmentation rate using the Ho:YAG laser is dependent on the size of ejected fragments. In addition, the Ho:YAG laser with the near infrared wavelength is insensitive to visible color of the urinary stones, as with biliary stone fragmentation (16) using the Ho:YAG laser.

C. Reflectivity of urinary stones for the Ho:YAG laser light

Table 10 shows the reflectivity of urinary stones and some biliary stones composed of 85 % cholesterol or more using the Ho:YAG laser at 3 W. We calculated the average value of the reflectivity of the stones in Table 11. The stones composed of cystine and uric acid had reflectivity less than 50 %, and those composed of calcite, COM, COD, TO, AAU, CP, CHPD, MAPH had reflectivity more than 50 % [see Fig. 10]. The reflectivity of the stone using the Ho:YAG laser might correspond to fragmentation rate to some extent. However, cystine had the lowest reflectivity among the urinary stones even though its fragmentation rate was lower than that of calcite. From visual observation of

the cystine stones using a stereomicroscope, the cystine stones produced relatively irregular shapes of particles when the fragmentation experiment was performed. On the other hand, the calcite stones collapsed, which looked like landslides. The fragment size of the calcite stones was generally bigger than that of the cystine stones. Thus, the reflectivity of the stone may not be related to the fragment size but to the chemical and structural components of the stone which influence the absorption of the laser energy, while the fragmentation rate may be somewhat depend on the fragment size. Figure 16 shows that the fragmentation rate of the stone may not depend on the reflectivity of the stone using the Ho:YAG laser. On the other hand, the fragmentation distance of the stone is inversely proportional to the reflectivity of the stone [see Fig. 17]. In addition, the fragmentation rate appears to refer to the hardness or the surface structure of the stone. We also performed reflectivity experiments for biliary stones (> 85 % cholesterol) using the Ho:YAG laser. The average reflectivity of the stones was approximately 50 % at the near infrared wavelength of the laser emission, which was roughly close to the one of the UA stones.

IV. DISCUSSION

We have investigated what represents the physical mechanisms emphasizing the interaction of Ho:YAG laser energy with urinary stones for laser lithotripsy. Our model is different from the one developed by Psihramis et al. to describe the mechanism of urinary stone fragmentation with the pulsed dye laser. They suggested that fragmentation of the stone may occur through the formation of a plasma at the stone surface which produces a shock wave that gradually fragments the stone. However, our model showed that urinary

stones begin to fragment by absorption of laser light by water, which induces a vapor bubble. Subsequent fractions of the laser pulse which pass through the vapor bubble are absorbed by the stone's surface. By the absorption of the laser energy, the cystine (m.p., 260 ° C) and UA stones are melted, and ejected stone fragments are swept away by the vapor bubble [see Table 12]. On the other hand, the stone composed of calcite fragmented as well as the ones composed of cystine or UA by the laser light, and the fragmentation rate of the calcite was also highest even if it was not melted by the laser light through the experiment using CH₃CN. It is not clear that the calcite stone fragmented whether by mechanical forces generated at the vapor - liquid boundary or by direct absorption of the laser energy by the stone creating thermal expansion of the stone by temperature rise. COM, COD, TO, AAU, CP, CHPD, MAPH was a little or hardly fragmented, as expected, because the reflectivity was more than 50 % for the laser light. Thus, it is clear that fragmentation of stones is dependent on the reflectivity of the stone for the laser energy and mechanical forces produced at the vapor - liquid boundary. Calculi composed of COD, MAPH, and UA fragment more easily than those composed of COM, cystine, and CP for the pulsed-dye laser lithotripsy. However, for the Ho:YAG laser lithotripsy, calculi composed of cystine, UA, and calcite are broken more easily than those composed of COM, COD, MAPH etc. [see Table 13]. Ho:YAG laser lithotripsy is different from pulsed-dye laser lithotripsy from the fact that the Ho:YAG laser can interact well with water, which induces a vapor bubble but the pulsed-dye laser can not. However, both techniques might be similar from the fact that the absorption of laser energy by urinary stones plays an important role in stone fragmentation. From the fact that the components of urinary stones vary with stones, the melting effect may be the result of

temperature rise by absorption of the laser light by the stone, which is sufficient to raise the temperature above the stone's melting point. In biliary stones, most stones melted by the Ho:YAG laser because the stones all contain cholesterol (17).

We have demonstrated that absorption of the laser light by the stone and the presence of a vapor bubble are both needed to fragment the stone effectively. The origin of the burning effect on the stone's surface and an accurate description of the mechanism of the vapor bubble to disperse the broken particle ejected from the stone requires further investigation.

<i>Threshold (mJ)</i>	<i>Wavelength (nm)</i>
For a MAPH calculus	
65.0 ± 4.2	577
54.1 ± 3.4	504
44.7 ± 3.6	445

Table 1. Fragmentation thresholds (mean ± standard deviation) vs wavelength in the pulsed-dye laser fragmentation. There is a fall in the fragmentation threshold on going from a longer to a shorter wavelength (11).

<i>Pulse duration (microseconds)</i>	<i>Threshold (mJ)</i>
For a Calcium Oxalate calculus	
1	83.1 ± 6.0
10	> 100
120	197.4 ± 41.5
300	264 ± 22.5

Table 2. Fragmentation thresholds vs pulse duration in the pulsed-dye laser fragmentation. The longer the pulse duration the greater the fragmentation threshold (11).

<i>Fiber diameter (Microns)</i>	<i>Threshold (mJ)</i>
For a Calcium Oxalate Calculus	
1000	130.8 ± 5.1
600	72.8 ± 2.0
400	32.1 ± 1.4
200	16.3 ± 0.6

Table 3. Fragmentation thresholds vs fiber diameter in the pulsed-dye laser fragmentation. The fiber diameter, which is also in effect the spot size of the laser energy on the stone, has a dramatic effect on the fragmentation threshold (11).

<i>Stone</i>	<i>Threshold fluence (J / cm²)</i>	
	<i>dye laser</i>	<i>Ho:YAG laser</i>
Cholesterol (white)	33.57 ± 4.50	20.14 ± 2.17
Light brown	13.68 ± 2.32	16.91 ± 1.83
Dark brown	6.22 ± 0.58	16.16 ± 1.75
Pigmented	1.99 ± 0.21	13.93 ± 1.53

Table 4. Fragmentation threshold values for different types of biliary stones. The visible wavelength of the dye laser produces stone fragmentation at lower fluences but the threshold values vary for different types of stones. However, the near infrared wavelength of the Ho:YAG laser requires higher fluence for efficient fragmentation but the threshold values are the same for all types of stones (16).

<i>Group number</i>	<i>Stone number</i>	<i>Predominant constituents</i>	
I	1 - 13, 15 - 20	calcium oxalate monohydrate	$\text{Ca}_2\text{O}_4 \bullet \text{H}_2\text{O}$
II	14	calcium oxalate dihydrate	$\text{Ca}_2\text{O}_4 \bullet 2\text{H}_2\text{O}$
III	21	tricalcium orthophosphate	$\text{Ca}_3(\text{PO}_4)_2$
IV	22	ammonium acid urate	$\text{NH}_4\text{H} \bullet \text{C}_5\text{H}_2\text{O}_3\text{N}_4 \bullet \text{H}_2\text{O}$
V	23	calcite	CaCO_3
VI	24 - 73	uric acid	$\text{C}_5\text{H}_4\text{N}_4\text{O}_3$
VII	74 - 75	calcium phosphate (carbonate form)	$\text{Ca}_{10}(\text{PO}_4 \bullet \text{CO}_3\text{OH})_6(\text{OH})_2$
VIII	76 - 84	calcium hydrogen phosphate dihydrate	$\text{CaHPO}_4 \bullet 2\text{H}_2\text{O}$
IX	85 - 94	cystine	$(\text{SCH}_2\text{CH}(\text{NH}_2)\text{--COOH})_2$
X	95 - 111	magnesium ammonium phosphate hexahydrate	$\text{MgNH}_4\text{PO}_4 \bullet 6\text{H}_2\text{O}$

Table 5. The list of urinary stones.

The urinary stones were classified by the predominant constituents of the stones.

<i>Stone type</i>	<i>Bubble size</i>
COM	0.77 ± 0.007
COD	0.81
TO	0.67
AAU	0.74
Calcite	0.70
UA	0.78 ± 0.011
CP	0.74 ± 0.002
CHPD	0.80 ± 0.004
Cystine	0.80 ± 0.01
MAPH	0.79 ± 0.006

Table 6. The list of average values of bubble size according to urinary stones while firing a series of 2 W pulses at a flash delay of 170 μ S.

- The tabulated values are mean \pm standard deviation.
- The unit is mm.

<i>Stones</i>	<i>Fragmentation distances (mm)</i>
COM	0.39 ± 0.006
COD	0.29 ± 0.003
TO	0.15 ± 0.005
AAU	0.30 ± 0.003
Calcite	0.78 ± 0.015
UA	0.87 ± 0.104
CP	0.29 ± 0.01
CHPD	0.16 ± 0.012
Cystine	0.89 ± 0.112
MAPH	0.21 ± 0.002

Table 7. Fragmentation distances of urinary stones using the Ho:YAG laser at a fixed power of 2 W (normal incidence case).

<i>Stone type</i>	<i>Description of fragmentation process</i>
COM	Moving the optical fiber close to the stone's surface while firing the laser, there were shallow holes on the stone's surface, producing fine dust. Subsequent firing of the laser caused the fine dust to disperse.
TO, MAPH, COD, CHPD	Repeating the experiment with the fiber moved close enough to the stone's surface, there was minor erosion of the stone's surface, generating fine dust. The stone was hardly fragmented by the laser energy.
AAU	When the fiber moved close enough to the stone's surface, the stone which had grains in one direction fragmented regardless of the direction of the grains. Subsequent laser pulses dispersed irregular fragments ejected by the laser.
Calcite	The absorption of the laser energy by the stone led to rapid fragmentation and collapse of the stone material from the surface. The collapse of the stone material looked like landslides.
UA	Similar to the fragmentation of the calcite stone, UA stone also fragmented readily, ejecting yellowish dust.
CP	Using the microscope technique, CP stone appeared to be composed of double shells which caused the fragmentation of the stone to be relatively difficult. By firing a series of laser pulses on the stone, there was some erosion on the stone's surface, producing filamentary material.
Cystine	The stone fragmented readily, ejecting irregular material from the surface.

Table 8. Description of fragmentation process of urinary stones using the Ho:YAG laser.

	<i>2W</i>	<i>5W</i>	<i>8W</i>
COM	0.022 ± 0.012	0.042 ± 0.032	0.040 ± 0.034
COD	0.149 ± 0.013	0.169 ± 0.022	0.186 ± 0.015
TO	0.039 ± 0.005	0.083 ± 0.048	0.056 ± 0.041
AAU	0.067 ± 0.039	0.084 ± 0.058	0.051 ± 0.042
Calcite	0.640 ± 0.303	0.787 ± 0.431	1.113 ± 0.600
UA	0.159 ± 0.083	0.301 ± 0.241	0.265 ± 0.138
CP	0.215 ± 0.039	0.220 ± 0.055	0.200 ± 0.097
CHPD	0.117 ± 0.063	0.081 ± 0.045	0.088 ± 0.042
Cystine	0.218 ± 0.050	0.246 ± 0.083	0.344 ± 0.148
MAPH	0.170 ± 0.070	0.257 ± 0.062	0.279 ± 0.072

Table 9. Fragmentation rates of urinary stones at fixed powers of 2,5, and 8 W for 15 seconds using the Ho:YAG laser.

- The tabulated values are mean ± standard deviation.
- The unit is mg / sec.

$V_2 (mV) / V_1 (mV)$ [STANDARD 99 % OF INTEGRATING SPHERE]	$V_2(mV) / V_1(mV)$ [STANDARD 10 % OF INTEGRATING SPHERE]	Stones	V_2 / V_1	Reflectivity
1.349 / 382.745	0.753 / 370.196	COM (1)	1.380 / 407.843	90.64 %
1.502 / 426.667	0.828 / 407.843	(2)	1.600 / 458.039	97.21 %
1.484 / 420.392	0.713 / 351.373	(3)	1.412 / 439.216	80.01 %
1.484 / 420.392	0.906 / 439.216	(6)	1.604 / 454.310	99.00 %
1.349 / 382.745	0.806 / 395.249	(7)	1.600 / 455.490	98.40 %
1.391 / 395.294	0.828 / 407.843	COD (14 A)	1.494 / 451.765	86.50 %
1.458 / 414.118	0.753 / 370.196	(14 B)	1.537 / 445.490	94.82 %
1.524 / 432.941	0.906 / 430.216	TO (21 A)	1.551 / 450.392	94.00 %
1.484 / 420.392	0.845 / 414.118	(21 A)	1.531 / 454.118	89.44 %
1.458 / 414.118	0.815 / 401.569	AAU (22 A)	1.412 / 445.490	78.09 %
1.391 / 395.294	0.753 / 370.196	(22 B)	1.380 / 426.667	81.70 %
1.349 / 382.745	0.906 / 439.216	CaCO ₃ (23 A)	1.223 / 414.118	64.25 %
1.502 / 426.667	0.713 / 351.373	(23 B)	1.129 / 389.020	61.97 %
1.519 / 426.657	0.828 / 407.843	(23 C)	1.035 / 370.190	54.21 %
1.349 / 382.745	0.806 / 395.249	UA (24)	1.004 / 375.098	49.01 %
1.391 / 395.294	0.845 / 414.118	(25)	1.067 / 396.275	49.62 %
1.502 / 426.667	0.815 / 401.569	(26)	1.004 / 386.275	44.14 %
1.484 / 420.392	0.753 / 370.196	(31)	1.129 / 432.196	44.75 %
1.458 / 414.118	0.713 / 351.373	(73)	1.223 / 432.196	58.16 %
1.349 / 382.745	0.909 / 439.215	CP (74)	1.286 / 395.294	82.43 %
1.391 / 395.295	0.759 / 370.194	(75)	1.317 / 376.471	97.79 %
1.391 / 395.294	0.808 / 395.239	CHPD (76)	1.223 / 370.196	85.77 %
1.524 / 432.941	0.845 / 414.118	(77)	1.341 / 432.941	73.74 %
1.349 / 382.745	0.758 / 370.193	(81)	1.286 / 395.294	82.65 %
1.502 / 426.667	0.828 / 407.843	(83)	1.380 / 395.294	97.20 %
1.484 / 420.392	0.725 / 357.186	(84)	1.380 / 407.843	90.10 %
1.458 / 414.118	0.759 / 370.194	Cystine (85)	0.944 / 432.941	19.08 %
1.306 / 395.294	0.815 / 401.569	(90)	0.941 / 389.020	37.33 %
1.349 / 382.745	0.713 / 351.373	(92)	0.941 / 376.471	38.07 %
1.502 / 426.667	0.906 / 439.216	(93)	0.941 / 414.118	22.80 %
1.484 / 420.392	0.828 / 407.843	(94)	0.941 / 420.392	22.46 %
1.396 / 395.294	0.713 / 351.373	MAPH (101)	1.312 / 414.118	77.64 %
1.349 / 382.745	0.815 / 401.569	(102)	1.367 / 414.118	85.86 %
1.519 / 426.657	0.845 / 414.118	(106)	1.204 / 414.118	60.94 %
1.458 / 414.118	0.819 / 401.568	(107)	1.172 / 420.392	55.10 %
1.349 / 382.745	0.753 / 370.196	(110)	1.198 / 395.294	69.73 %
1.391 / 395.294	0.906 / 439.216	Cholesterol (123)	1.192 / 420.392	58.16 %
1.458 / 414.118	0.815 / 401.569	Cholesterol (124)	0.941 / 389.020	43.82 %

Table 10. Reflectivity of urinary and biliary stones at a fixed laser power of 3 W.

<i>Stones</i>	<i>Average reflectivity (%)</i>
Calcium Oxalate Monohydrate	93.05
Calcium Oxalate Dihydrate	90.66
Tricalcium Orthophosphate	91.72
Ammonium Acid Urate	79.90
Calcite	60.14
Uric Acid	49.14
Calcium Phosphate	90.11
Calcium Hydrogen Phosphate Dihydrate	85.89
Cystine	27.95
Magnesium Ammonium Phosphate Hexahydrate	69.85

Table 11. Average reflectivity of urinary stones for the Ho:YAG laser light at a fixed power of 3W.

Laser light is emitted
from the optical fiber tip



Some laser light is absorbed by water
to form vapor bubble; remainder
of laser light is absorbed or reflected by stone surface



Cystine and UA stones are melted,
ejected fragments are resolidified,
and swept away by the vapor bubble

Other stones are not melted but
fragmented by direct absorption
of the laser light by the stone
inducing thermal expansion of the
stone or mechanical forces at the
vapor-liquid boundary of the vapor
bubble

Table 12. Fragmentation mechanism of urinary stones using the Ho:YAG laser

<i>pulsed-dye laser</i>	<i>Ho:YAG laser</i>
<p>Urinary stone fragmentation depends on the absorption of the laser energy by the stone and power density, which refers to the hardness of the stone and the characteristics of the stone's surface. Fragmentation rate depends on the component and size of the calculi.</p>	<p>Urinary stone fragmentation depends on the absorption of the laser energy by the stone, which refers not to the laser power but to the stone's component, and the distance between the fiber tip and the stone's surface. Therefore, it is clear that the stone fragmentation depends on the reflectivity of the laser energy by the stone and mechanical forces generated at the vapor - liquid boundary of the vapor bubble. Fragmentation rate is dependent on the size of ejected fragments which refers to hardness or surface structure of the stone.</p>
<p>COD, MAPH, UA stones fragment more easily than COM, Cystine, CP stones.</p>	<p>Cystine, UA, Calcite stones fragment more easily than COM, COD, MAPH stones.</p>
<p>Plasma formation at the stone's surface leads to fragmentation of the stone.</p>	<p>Vapor bubble formation in water serves to fragment the stone.</p>
<p>The visible wavelength of the pulsed-dye laser is sensitive to visible color of the stones. Stones with a dark surface fragment well, whereas those with a pale, reflective surface fragment poorly.</p>	<p>The near infrared wavelength of the Ho:YAG laser is insensitive to visible color of the stones.</p>

Table 13. Comparison of urinary stone fragmentation using the pulsed-dye and Ho:YAG lasers.

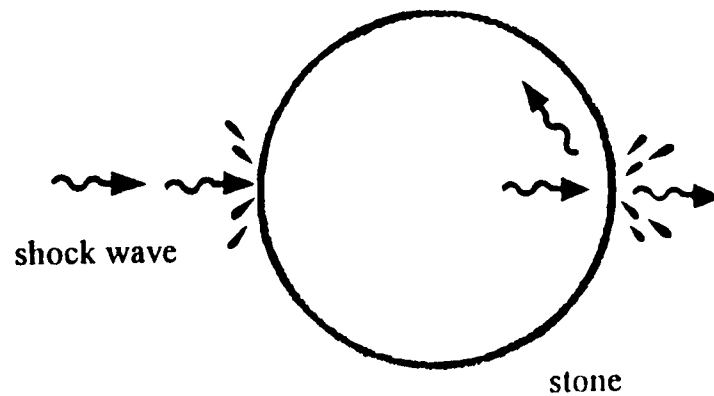


Figure 1. Schematic representation of stone fragmentation using extracorporeal shock wave lithotripsy devices. The contact of a shock wave with a stone produces a compression wave along the front surface of the stone, causing the anterior surface to crumble. As the shock wave traverses to the posterior surface of the stone, the wave is partially reflected, creating tensile stress and fragmentation along this surface.

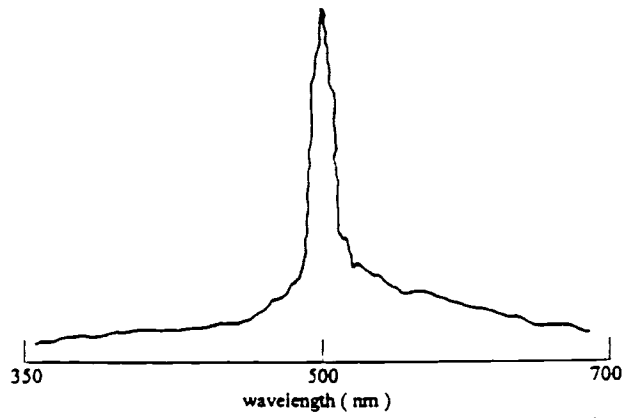


Figure 2. Spectrum from a cystine stone (11).

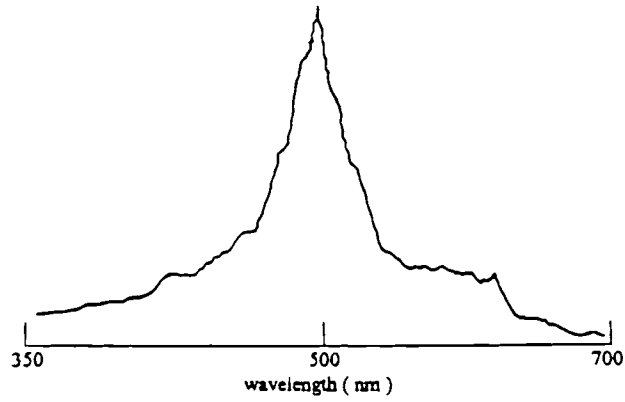


Figure 3. Spectrum from a CHPD stone (11).

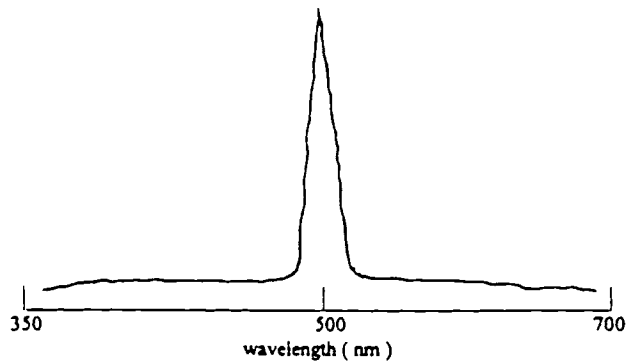


Figure 4. Spectrum showing reflection of pulsed dye laser light from a surface of a stone (11).

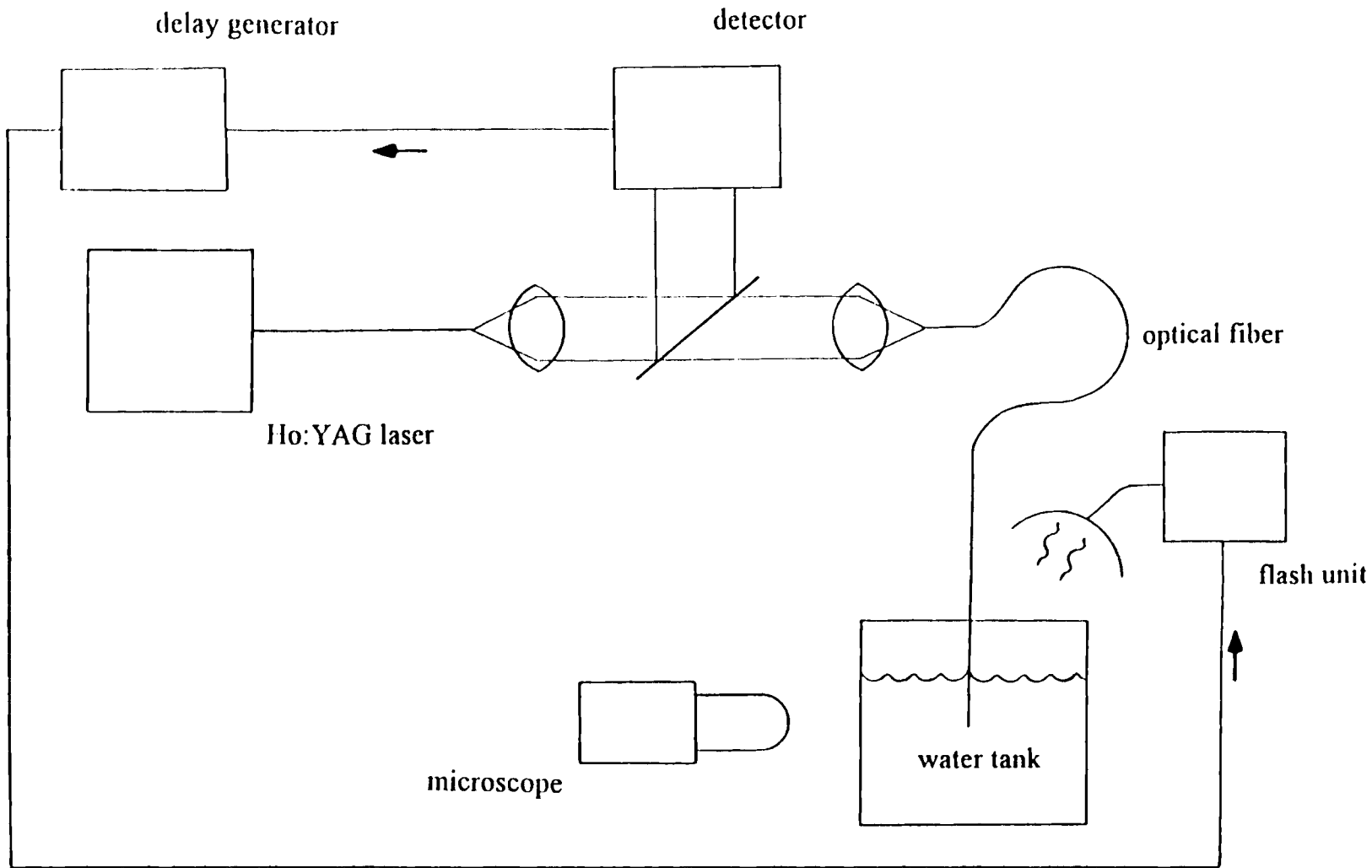


Figure 5. Schematic illustration of the equipment of visual observation.

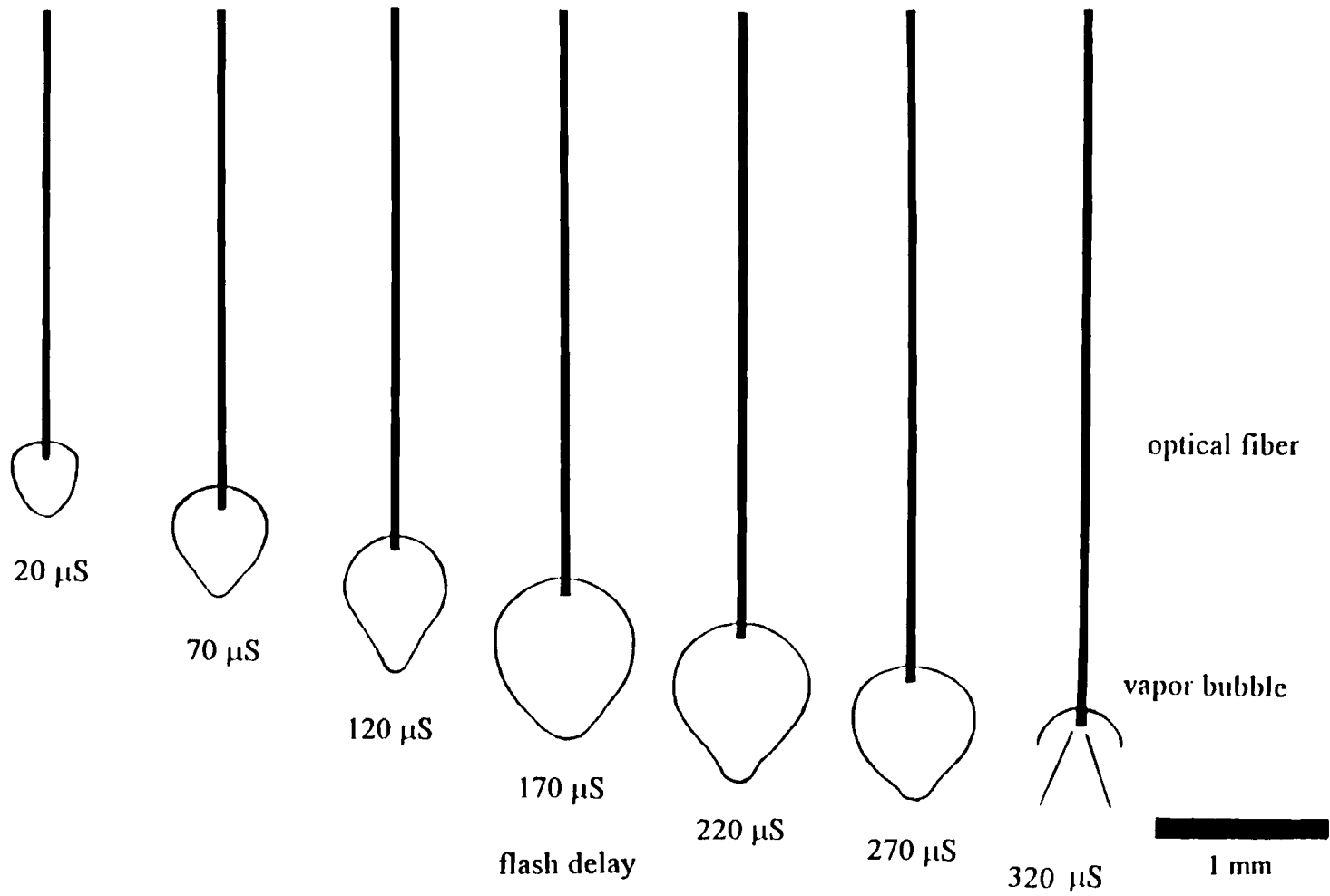


Figure 6. The evolution of vapor bubbles at 2 W pulses while varying the lengths of delay (20 μS - 320 μS).

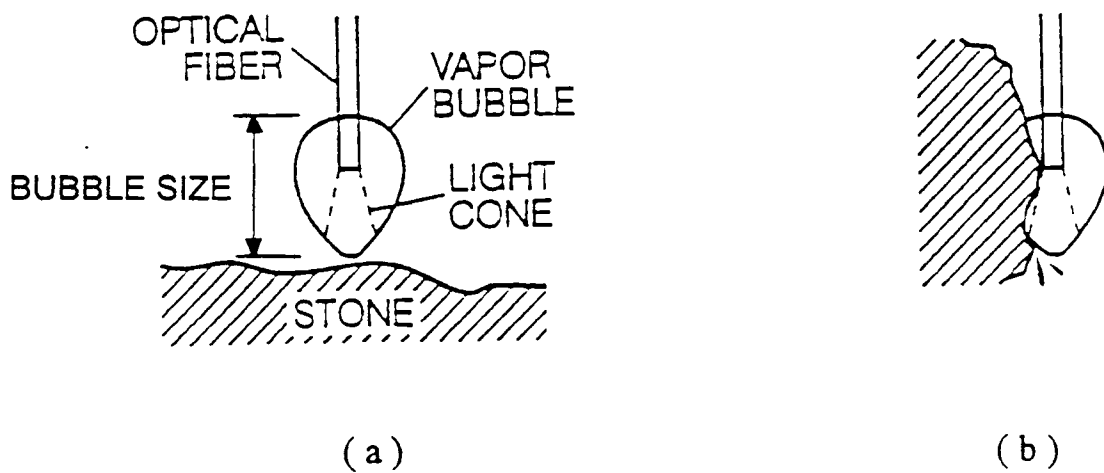


Figure 7. Schematic representation of stone ablation with the Ho:YAG laser. (a) Normal incidence (b) Tangential incidence.

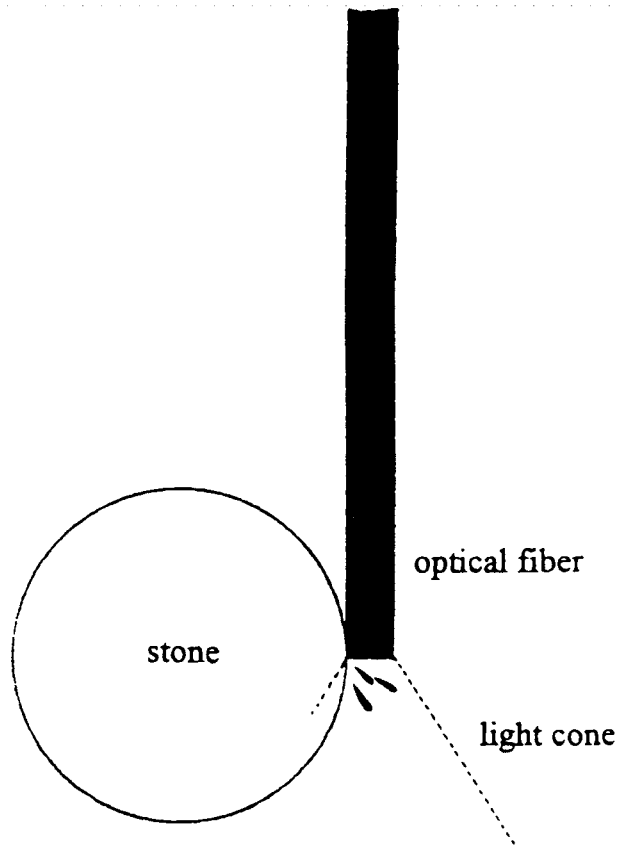


Figure 8. Schematic representation of stone ablation in tangential incidence.

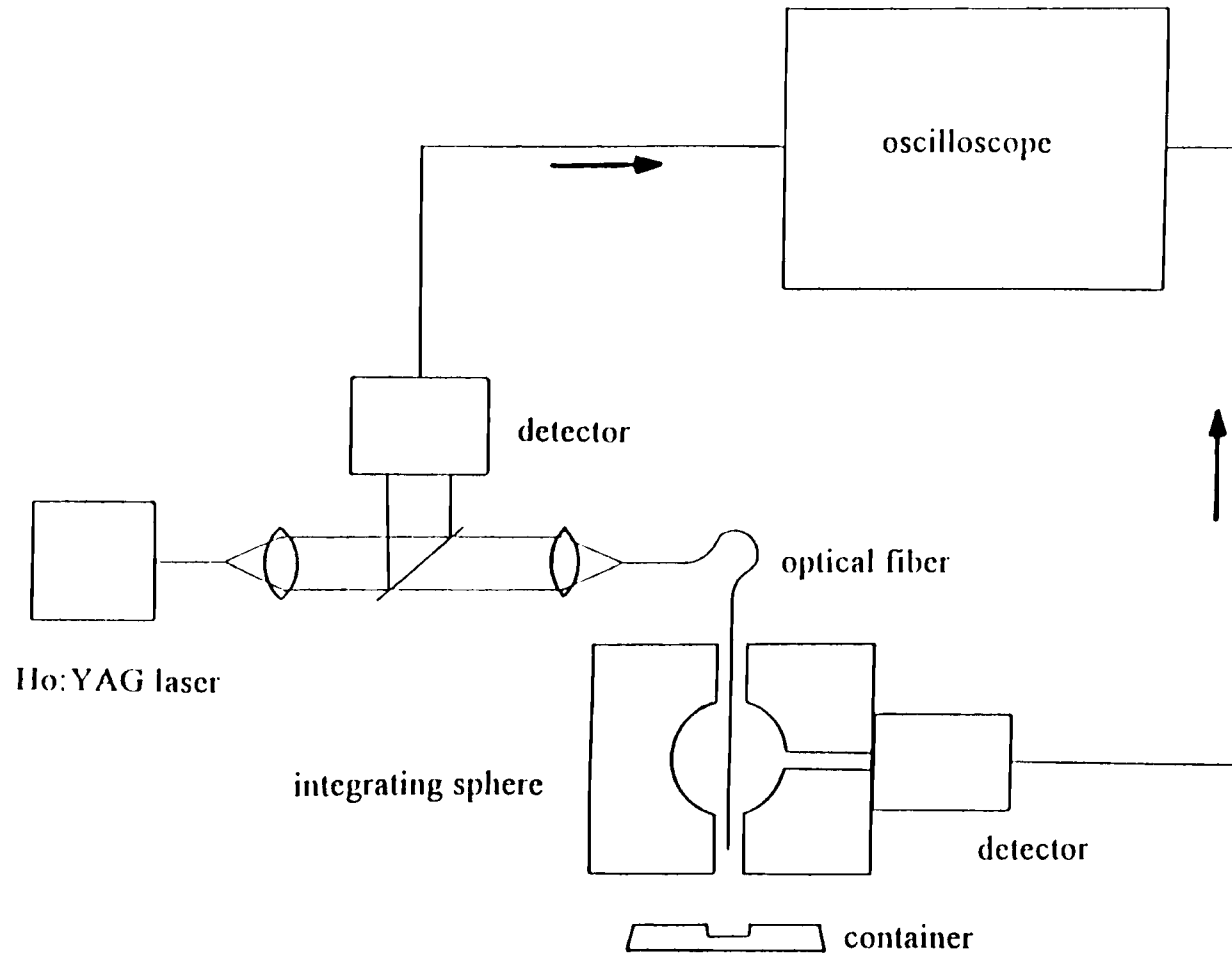


Figure 9. Schematic illustration of the reflectivity apparatus.

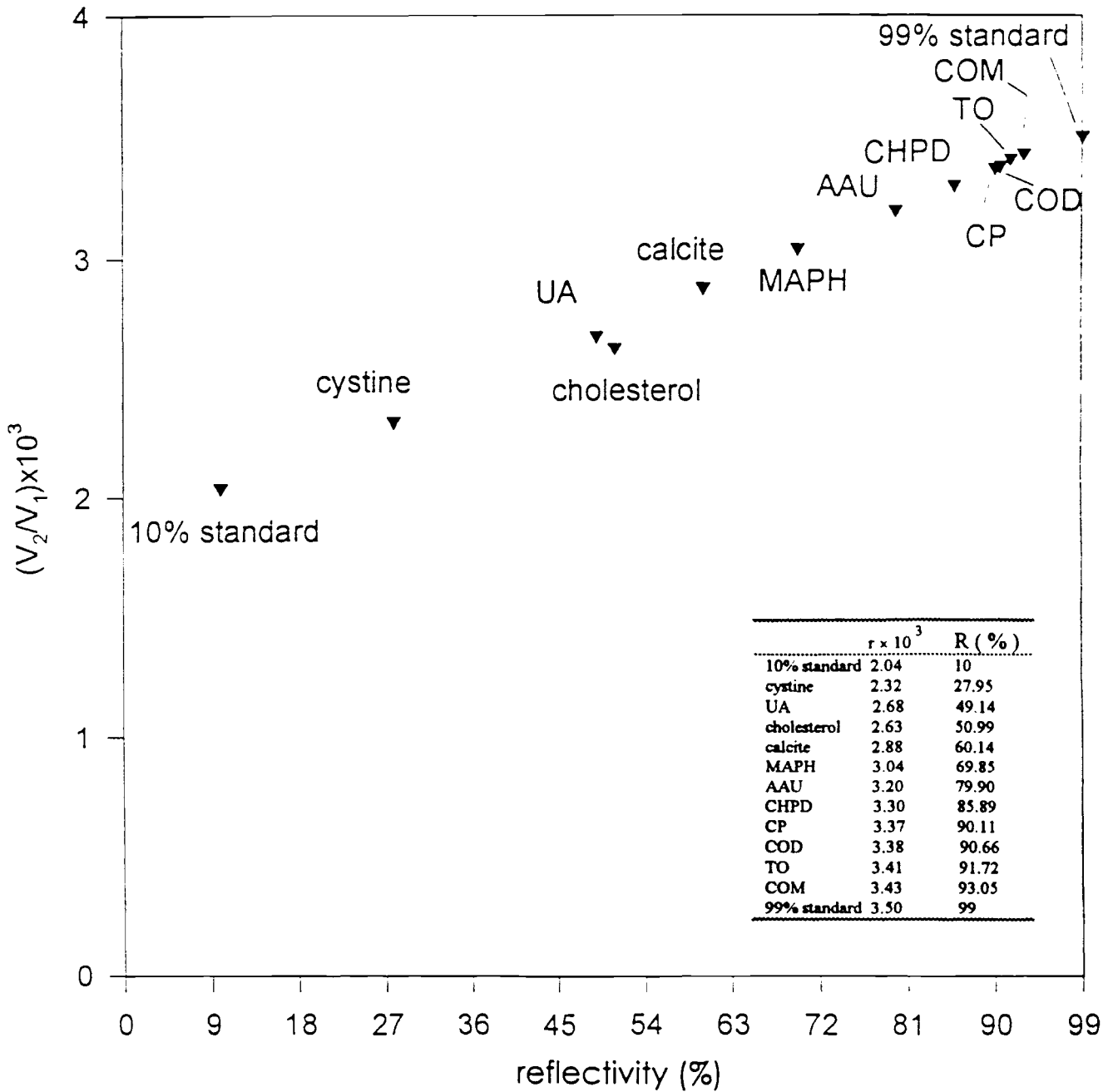


Figure 10. The reflectivity of urinary and biliary stones (> 80 % cholesterol) lied between 10 % and 99 % for the Ho:YAG laser light ($V_2 / V_1 = r$).

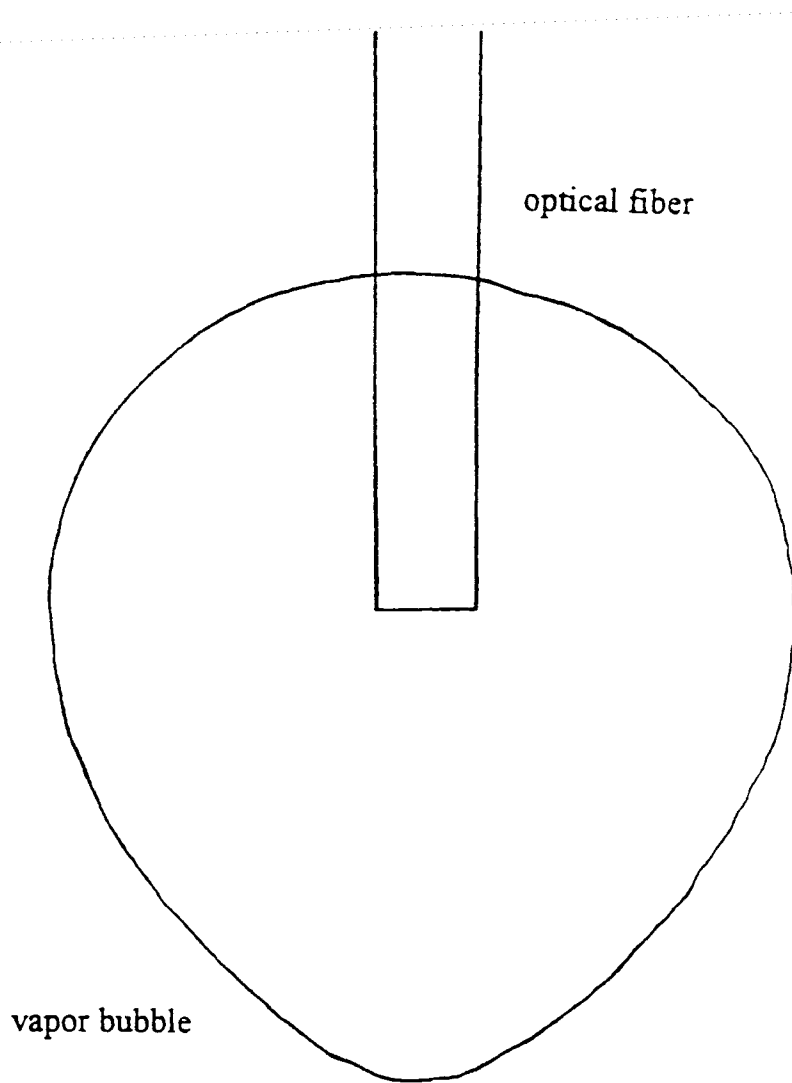


Figure 11. Schematic representation of a typical Ho:YAG laser-induced vapor bubble in water at a flash delay of 170 μ S.

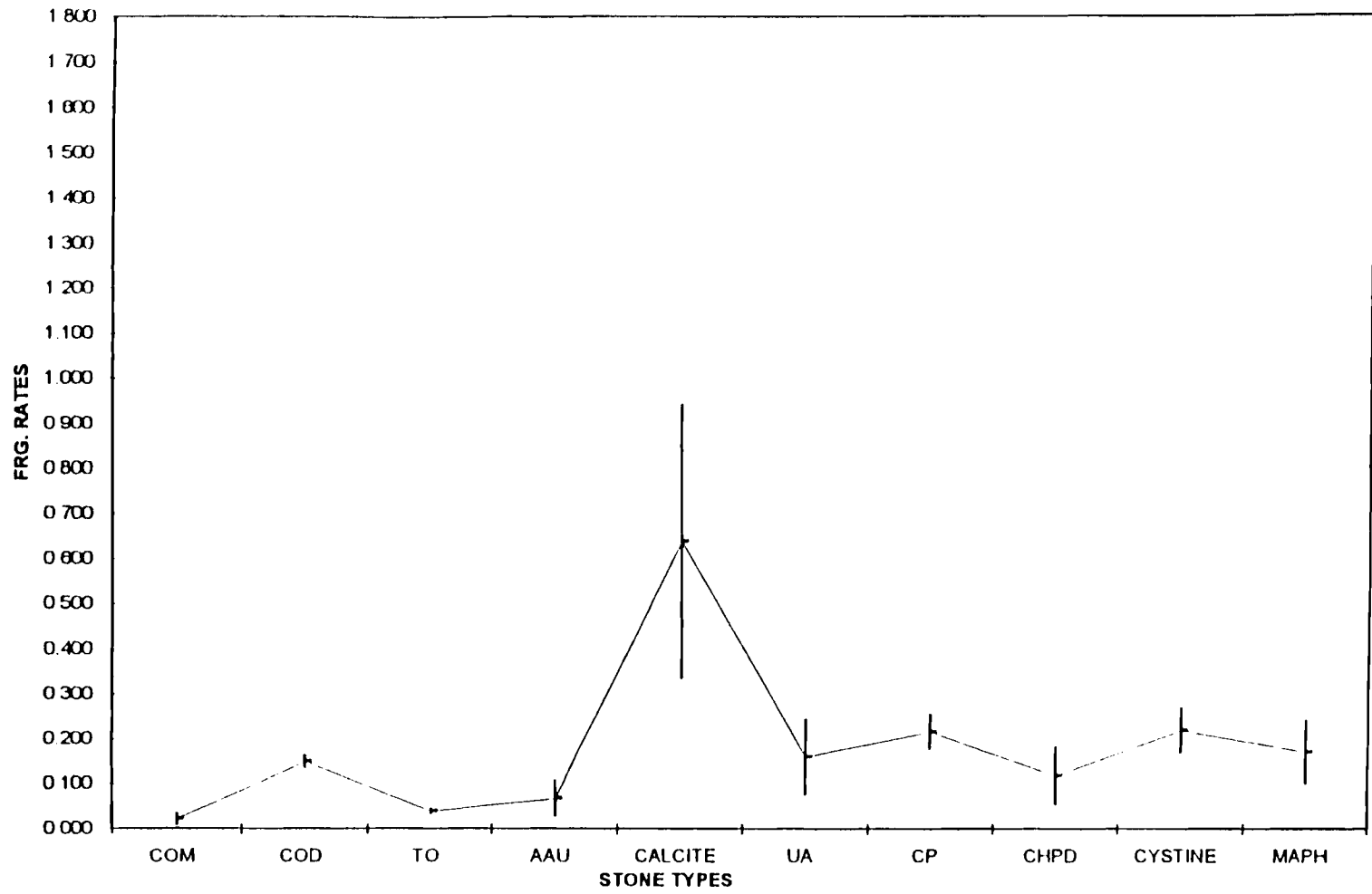


Figure 12. Fragmentation rate of urinary stones at a pulse repetition rate of 15 Hz and a fixed power of 2 W for 15 seconds.

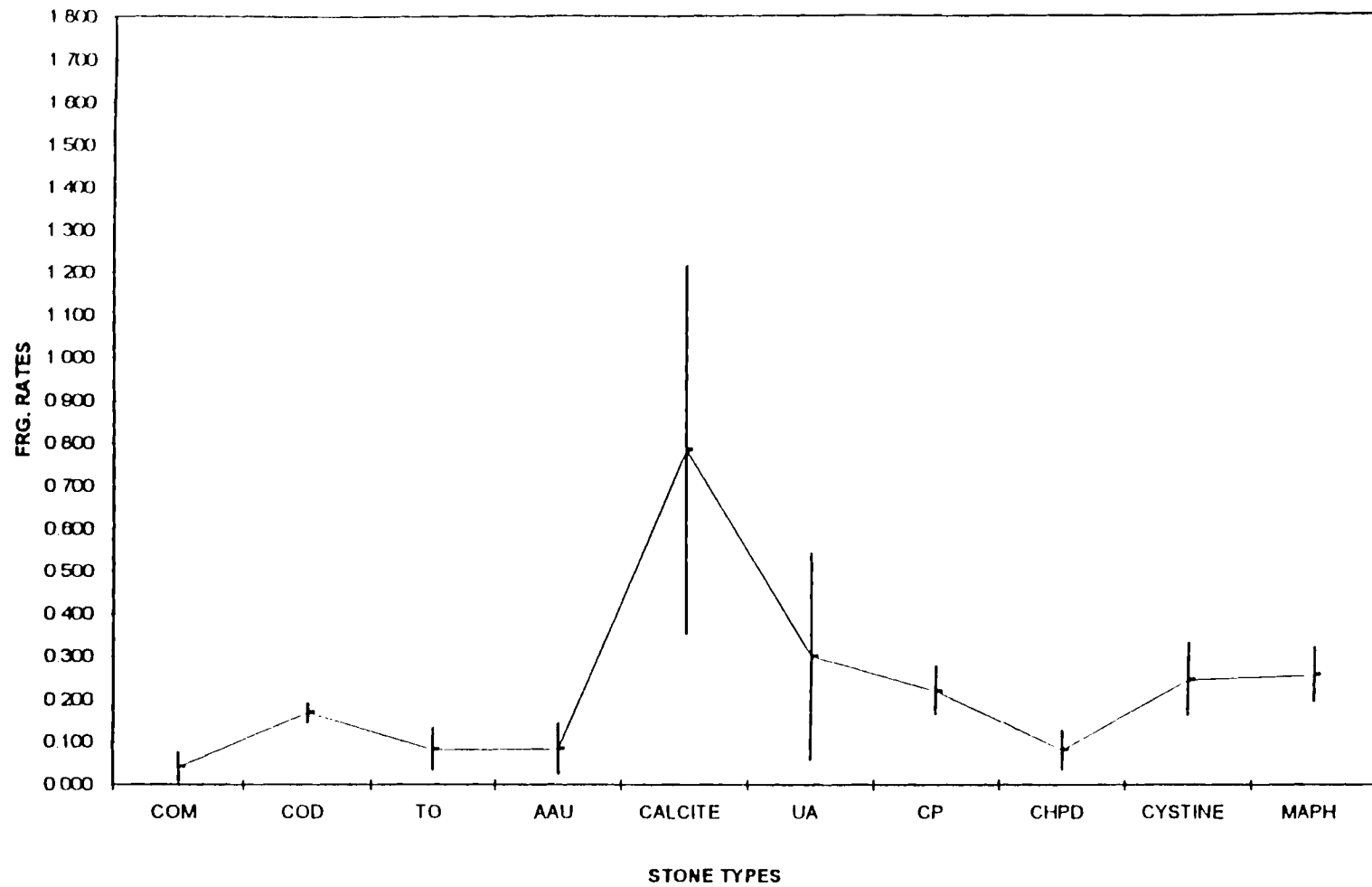


Figure 13. Fragmentation rate of urinary stones at a pulse repetition rate of 15 Hz and a fixed power of 5 W for 15 seconds.

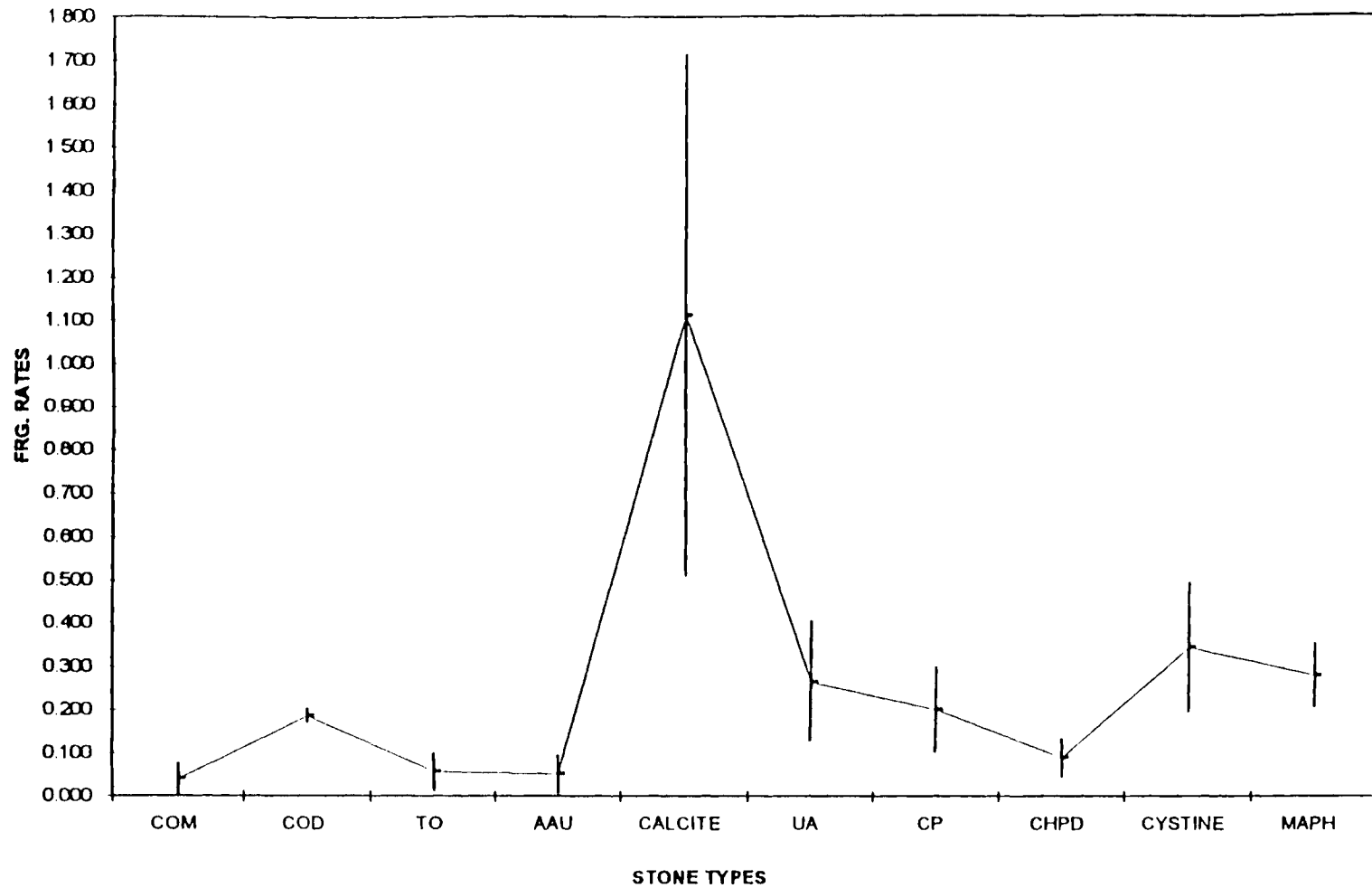


Figure 14. Fragmentation rate of urinary stones at a pulse repetition rate of 15 Hz and a fixed power of 8 W for 15 seconds.

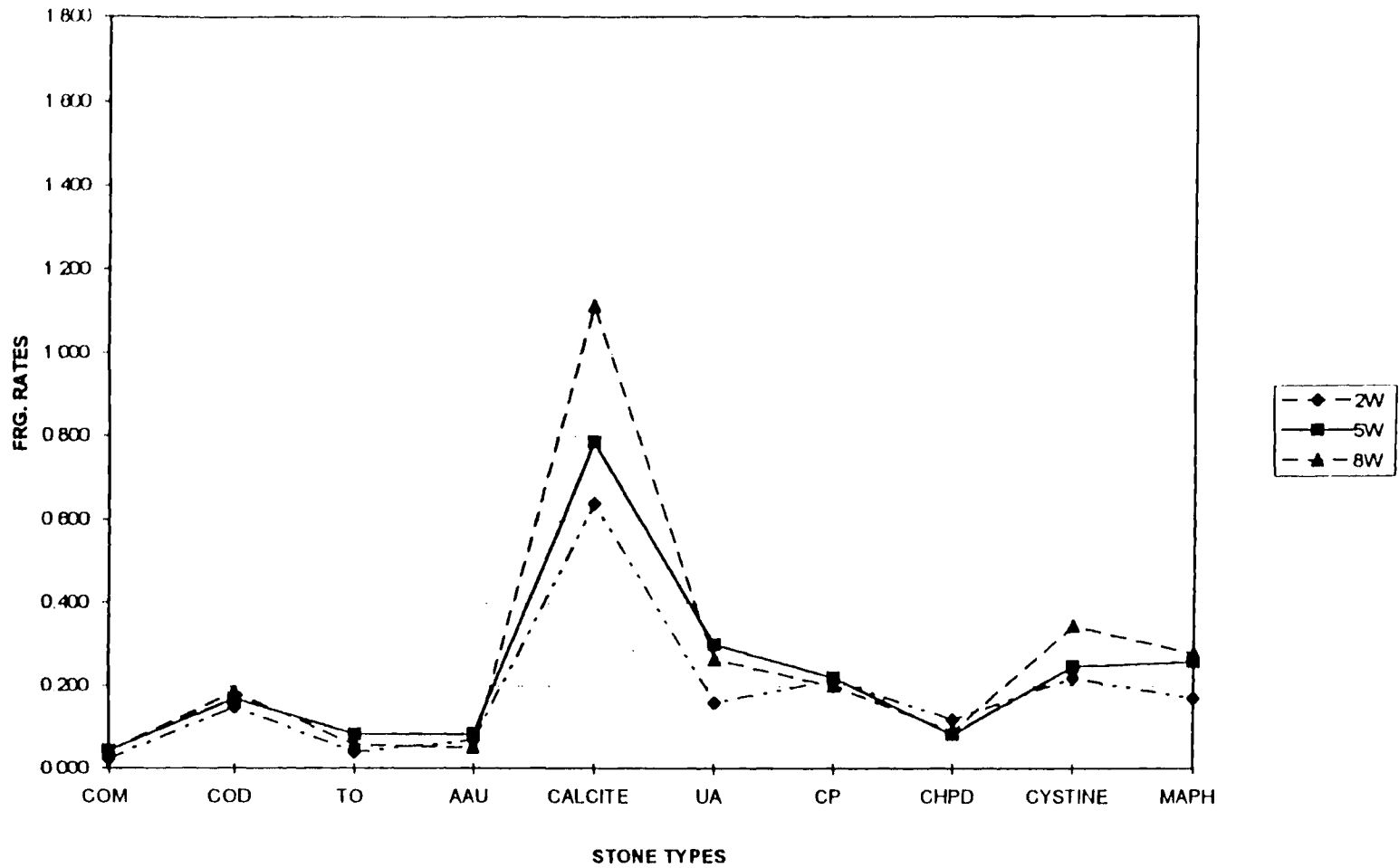


Figure 15. Fragmentation rate of urinary stones at a pulse repetition rate of 15 Hz and fixed powers of 2, 5, 8 W for 15 seconds.

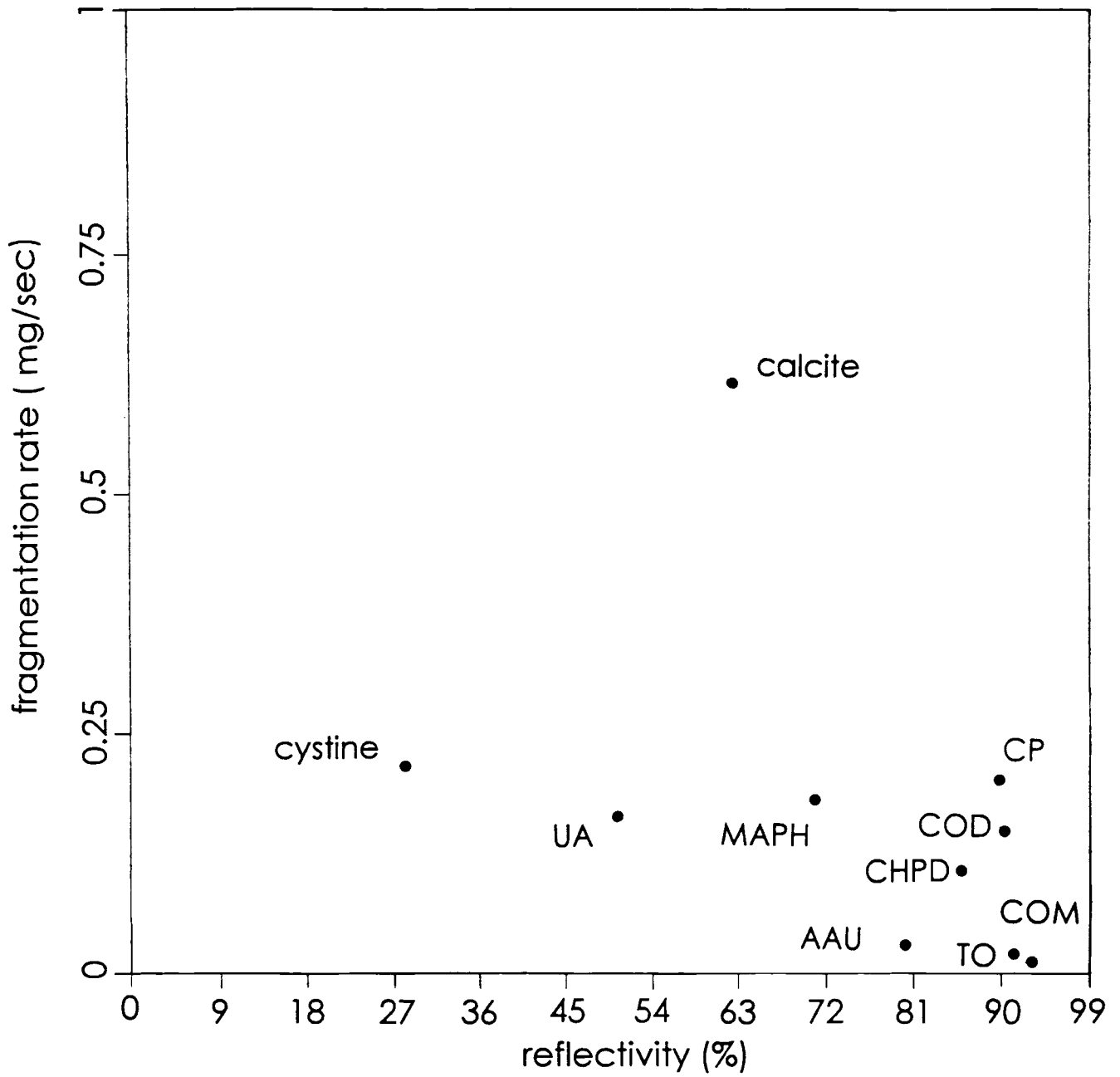


Figure 16. Comparisons of the fragmentation rate and the reflectivity of urinary stones using the Ho:YAG laser.

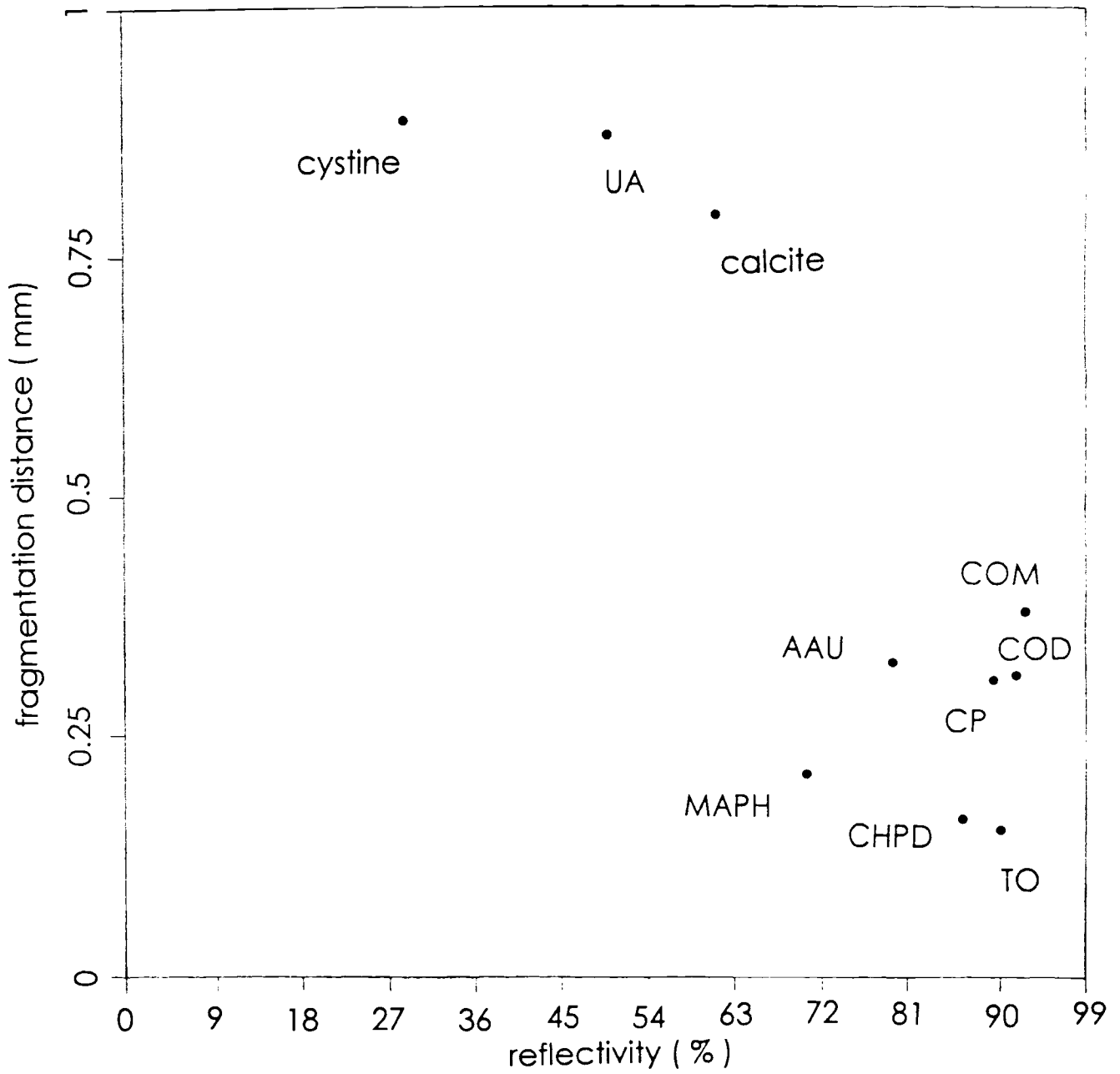


Figure 17. Comparisons of the fragmentation distance and the reflectivity of urinary stones using the Ho:YAG laser.

REFERENCES

1. Kim, K. M.; Resau, J.; Chung, J. Scanning electron microscopy of urinary stone as a diagnostic tool. *Journal of Scanning Electron Microscopy* 4: 1819-1831; 1984.
2. Lehtoranta, K.; Salo, J.; Lindell, O.; Lehtonen, T. Treatment of urinary stones by extracorporeal shock wave lithotripsy. *Journal of Annales Chirurgiae et Gynaecologiae* 82: 90-96; 1993.
3. Tanagho, E. A.; Mcaninch, J. W. *General Urology* 12: 1-706; 1988.
4. Daudon, M.; Bader, C. A.; Jungers, P. Urinary calculi: review of classification methods and correlations with etiology. *Journal of Scanning Microscopy* 7 (3): 1081-1106; 1993.
5. Daudon, M. Morphoconstitutional classification of urinary stones. *Journal of Urolithiasis* 1989.
6. Wilson, W. T.; Preminger, G. M. Extracorporeal shock wave lithotripsy. *Journal of Urologic Clinics of North America* 17 (1): 231-239; 1990.
7. Foo, K. T.; Wujanto, R.; Wong, M. Y. C. Laser lithotripsy for ureteric stones. *Journal of Annals Academy of Medicine* 23 (1): 43-45; 1994.
8. Psihramis, K. E.; Buckspan, M. B. Laser lithotripsy in the treatment of ureteral calculi. *Journal of Canada Medical Association* 142 (8): 833-835; 1990.
9. Murray, A.; Basu, R; Fairclough, P. D.; Wood, R. F. M. Gallstone lithotripsy with the pulsed dye laser: in vitro studies. *British Journal of Surgery* 76: 457-460; 1989.

10. Borirakchanyavat, S.; Puliafito, C. A.; Kliman, G. H.; Margolis, T. I.; Galler, E. L. Holmium-YAG laser surgery on experiment vitreous membranes. *Journal of Arch Ophthalmol* 109: 1605-1609; 1991.
11. Watson, G.; Murray, S.; Dretler, S. P.; Parrish, J. A. The pulsed dye laser for fragmentating urinary calculi. *The Journal of Urology* 138: 195-198; 1987.
12. Cancellieri, G. Single-mode optical fiber measurement: characterization and sensing: 1-337; 1993.
13. Holden, D.; Whitehurst, C.; Rao, P. N.; King, T. A.; Blacklock, N. J. Identification of urinary stone composition by pulsed dye laser. *British Journal of Urology* 65: 441-445; 1990.
14. Nelson, J. B.; Graham, J. B. Lithotripsy of urinary calculi by tunable pulsed dye lasers: A randomized in vitro study. *The Journal of Urology* 151: 656-659; 1994.
15. Dretler, S. P. Stone fragility-a new therapeutic distinction. *The Journal of Urology* 139: 1124; 1988.
16. Spindel, M. L.; Moslem, A.; Bhatia, K. S.; Jassemnejad, B.; Bartels, K. E.; Powell, R. C.; O'Hare, C. M.; Tytle, T. Comparison of holmium and flashlamp pumped dye lasers for use in lithotripsy of biliary calculi. *Journal of Lasers in Surgery and Medicine* 12: 482-489; 1992.
17. Schafer, S. A.; Durville, F. M.; Jassemnejad, B.; Bartels, K. E.; Powell, R. C. Mechanisms of biliary stone fragmentation using the Ho:YAG laser. *IEEE Journal of*

- Transactions on Biomedical Engineering 41 (3): 276-283; 1994.
18. Teng, P; Nishioka, N. S.; Anderson, R. R.; Deutsch, T. F. Optical studies of pulsed laser fragmentation of biliary calculi. *Journal of Applied Physics*. B42: 73-78; 1987.
 19. Acoustic studies of the role of immersion in plasma-mediated laser ablation. *IEEE Journal of Quantum Electron* 23: 1845-1852; 1987.
 20. Hale, G. M.; Querry, M. R. Optical constants of water in the 200 nm to 200 μm wavelength region. *Journal of Applied Optics* 12: 555-563; 1973.
 21. Pouchert, C. J. *The Aldrich Library of Infrared Spectra* III 1: 561; 1981.
 22. Lee, Y. H.; Chen, M. T.; Huang, J. K.; Chang, L. S. Analysis of urinary calculi by infrared spectroscopy. *Journal of China Medicine* 45: 157-165; 1990.
 23. Celebrating 100 years of integrating sphere technology. *Catalog of Labsphere*.
 24. Lo, E. Y.; Petschek, H.; Rosen, D. I. A hydrodynamic model for the laser-induced fragmentation of calculi. *Journal of Lasers in the Life Science* 3 (4): 233-244; 1990.

VITA

Jong-Eul LEE

Candidate for the Degree of

Master of Science

**Thesis: MECHANISMS OF URINARY STONE FRAGMENTATION
 USING THE HO:YAG LASER**

Major Field: Physics

Biographical:

**Personal Data: Born in Dongsung-Dong, Seoul, On June 22, 1965, the son of
 Kyu-Ho LEE and Jeong-Jie SHIN.**

**Education: Graduated from Yangchung High School, Seoul, Korea in March 1984;
 received Bachelor of Science degree in Physics from Dongguk University,
 Seoul, Korea in February 1991. Completed the requirements for the Master of
 Science degree with a major in Physics at Oklahoma State University in
 December 1995.**

**Experience: Employed by Oklahoma State University, Department of Physics as a
 graduate research assistant: Oklahoma State University, Department of Physics
 1994 to present.**